Supporting Information

Table of Content

NMR spectra and MS data 2
Computational Chemistry 14
Electrochemistry 21
Electrochemical data of **[C0]$^{2+}$** 21
Electrochemical data of **[C1]$^{2+}$** 22
Electrochemical data of **[C2]$^{2+}$** 24
Cyclic voltammetry of **[H$_2$-L0]$^{2+}$**, **[H$_2$-L1]$^{2+}$** and **[H$_2$-L2]$^{2+}$** 26
Cyclic voltammetry of anthracene and pyrene 27
Spectroelectrochemical data of **[C1]$^{2+}$** 28
Spectroelectrochemical data of **[C2]$^{2+}$** 29
Luminescence Properties 30
Singlet Oxygen Experiments 33
References 34

NMR spectra and MS data

4-(anthracen-9-yl)-2,6-dichloropyridine **2-1**:

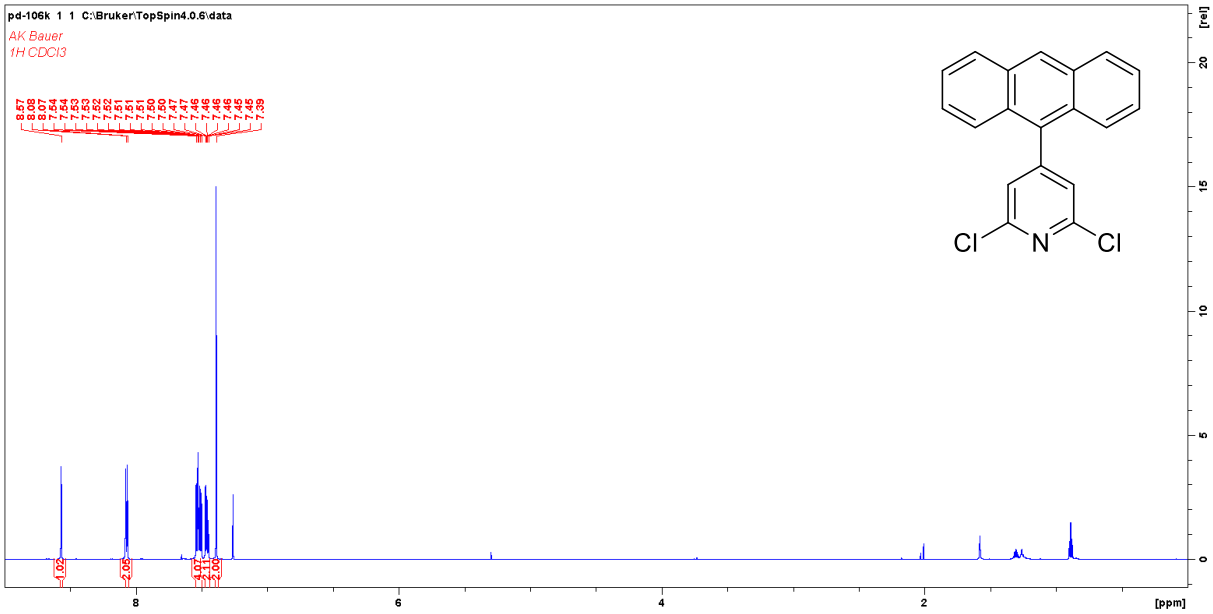

*Figure S 1: ^{1}H-NMR of 4-(anthracen-9-yl)-2,6-dichloropyridine **2-1** in $CDCl_3$.*

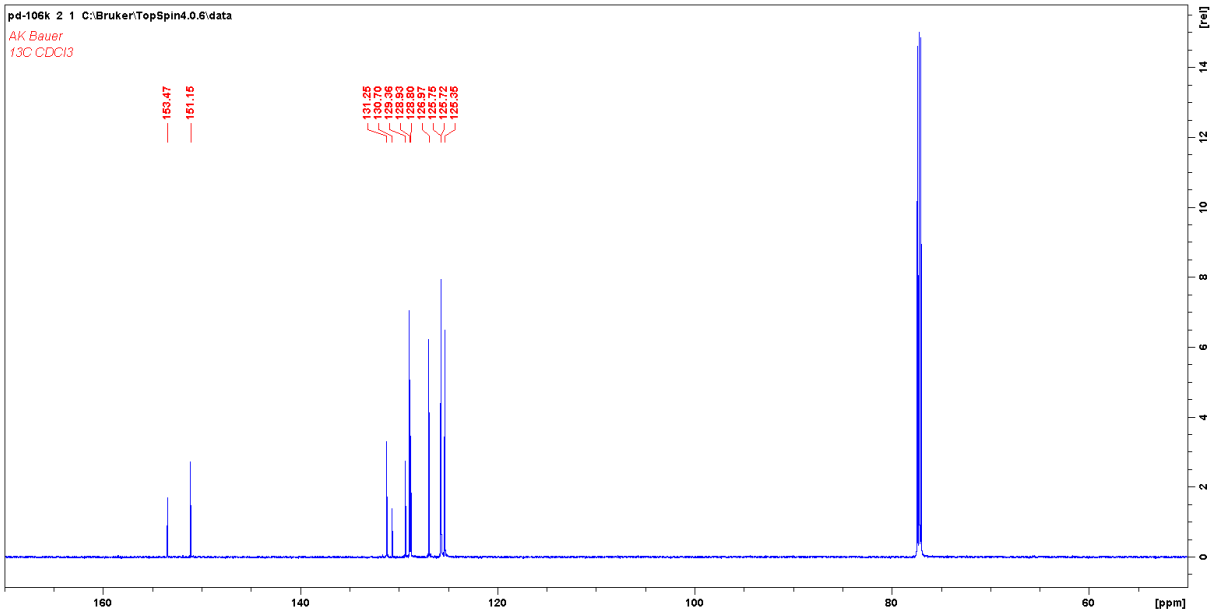

*Figure S 2: ^{13}C-NMR of 4-(anthracen-9-yl)-2,6-dichloropyridine **2-1** in $CDCl_3$.*

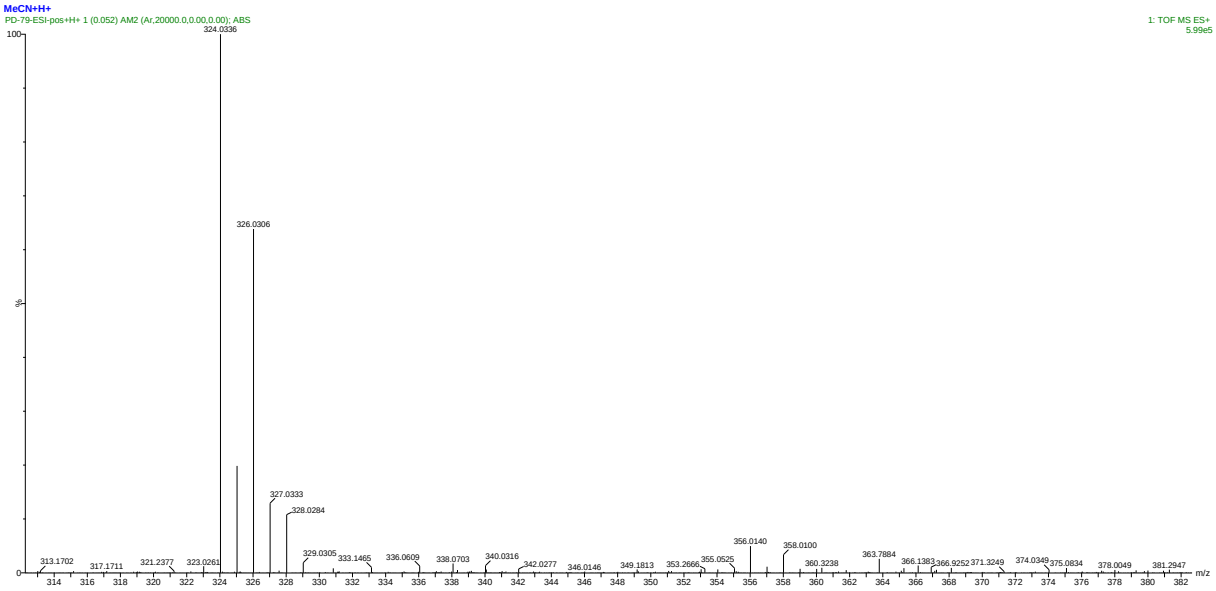

*Figure S 3: ESI-MS of 4-(anthracen-9-yl)-2,6-dichloropyridine **2-1** in MeCN.*

2,6-dichloro-4-(pyren-1-yl)pyridine **2-2**:

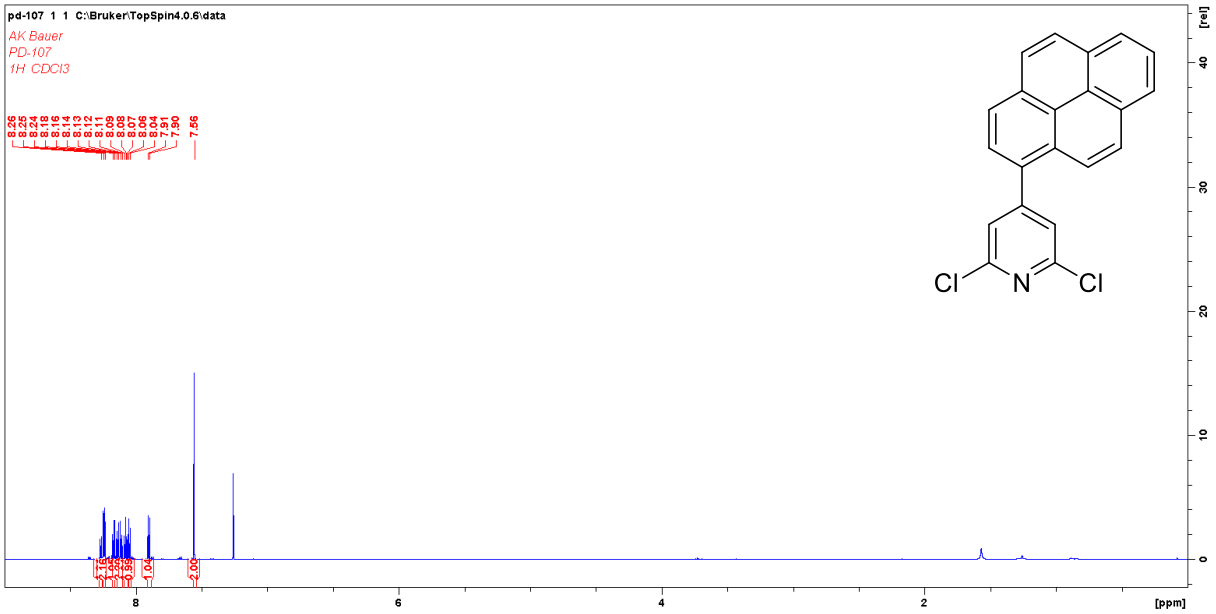

*Figure S 4: ^{1}H-NMR of 2,6-dichloro-4-(pyren-1-yl)pyridine **2-2** in $CDCl_3$.*

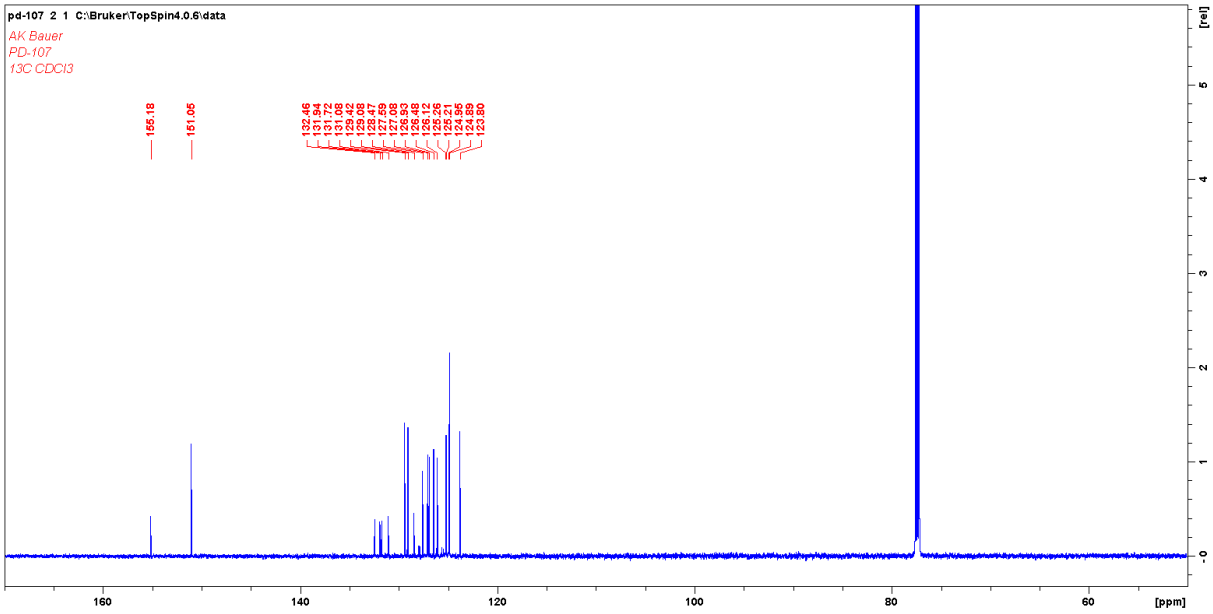

*Figure S 5: ^{13}C-NMR of 2,6-dichloro-4-(pyren-1-yl)pyridine **2-2** in $CDCl_3$.*

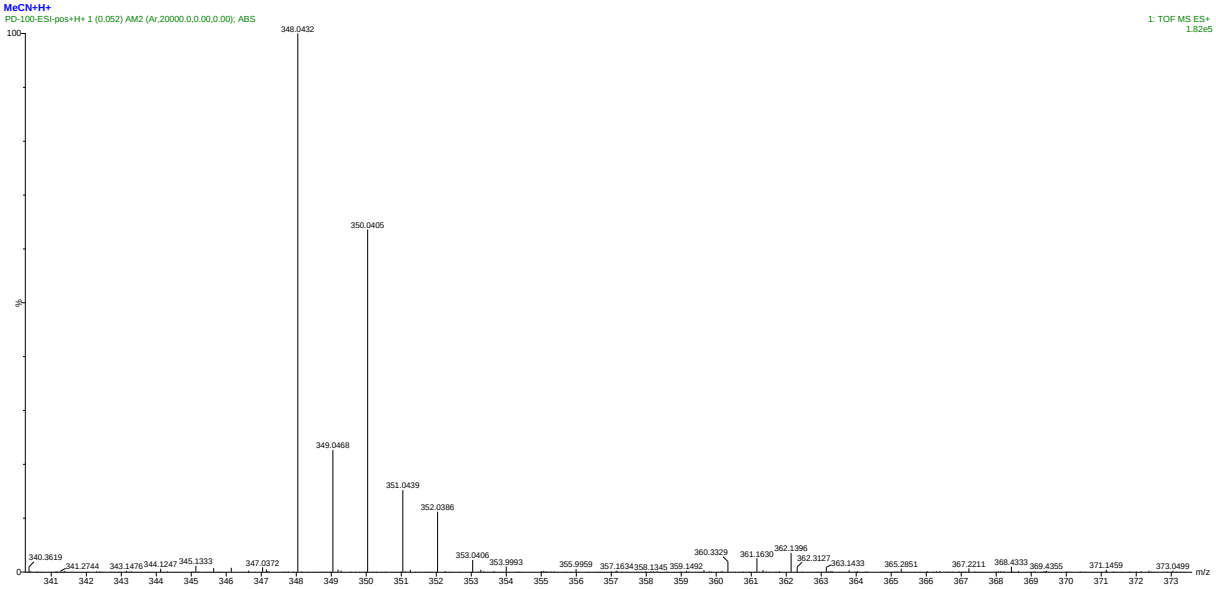

*Figure S 6: ESI-MS of 2,6-dichloro-4-(pyren-1-yl)pyridine **2-2** in MeCN.*

4-(anthracen-9-yl)-2,6-di(1*H*-imidazol-1-yl)pyridine **3-1**:

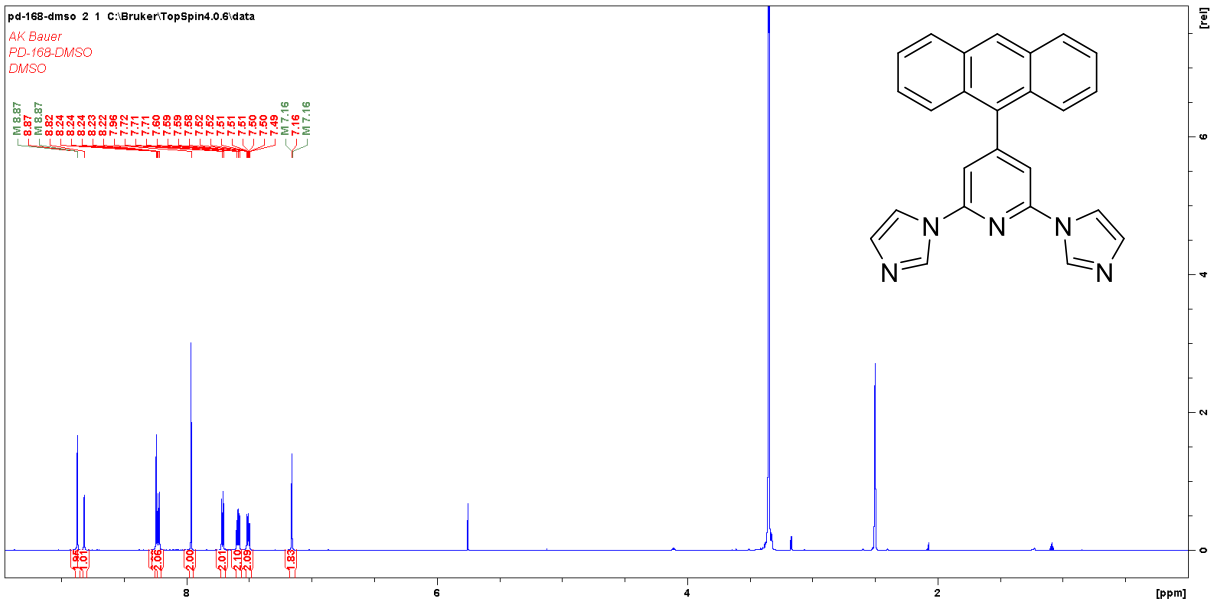

*Figure S 7: ^{1}H-NMR of 4-(anthracen-9-yl)-2,6-di(1*H*-imidazol-1-yl)pyridine **3-1** in d_6-DMSO.*

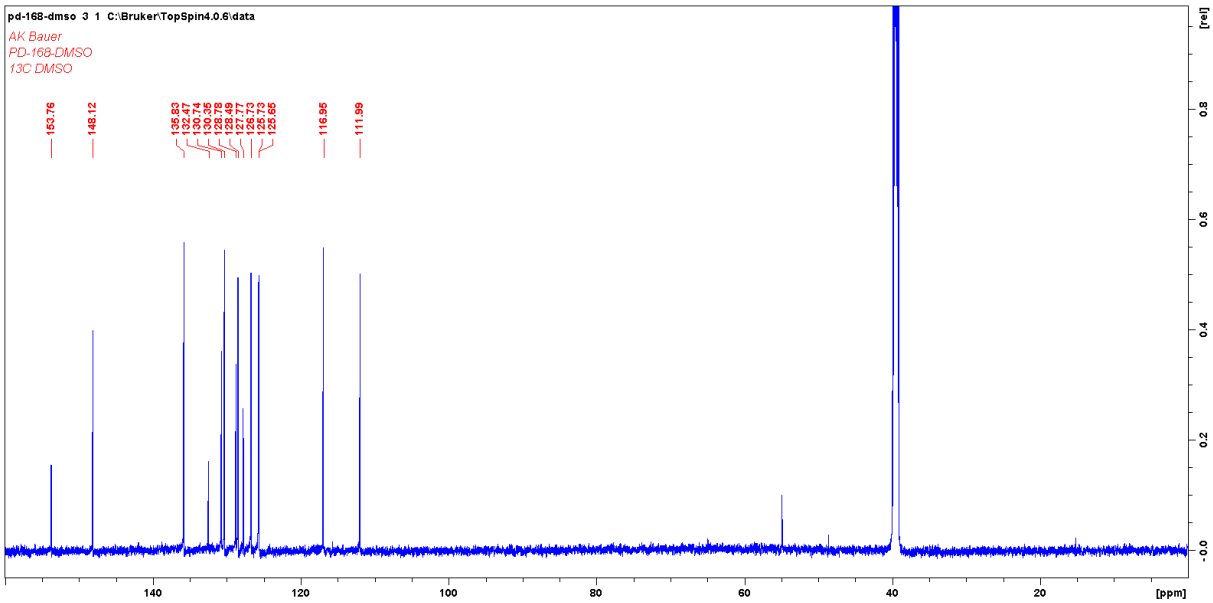

*Figure S 8: ^{13}C-NMR of 4-(anthracen-9-yl)-2,6-di(1*H*-imidazol-1-yl)pyridine **3-1** in d_6-DMSO.*

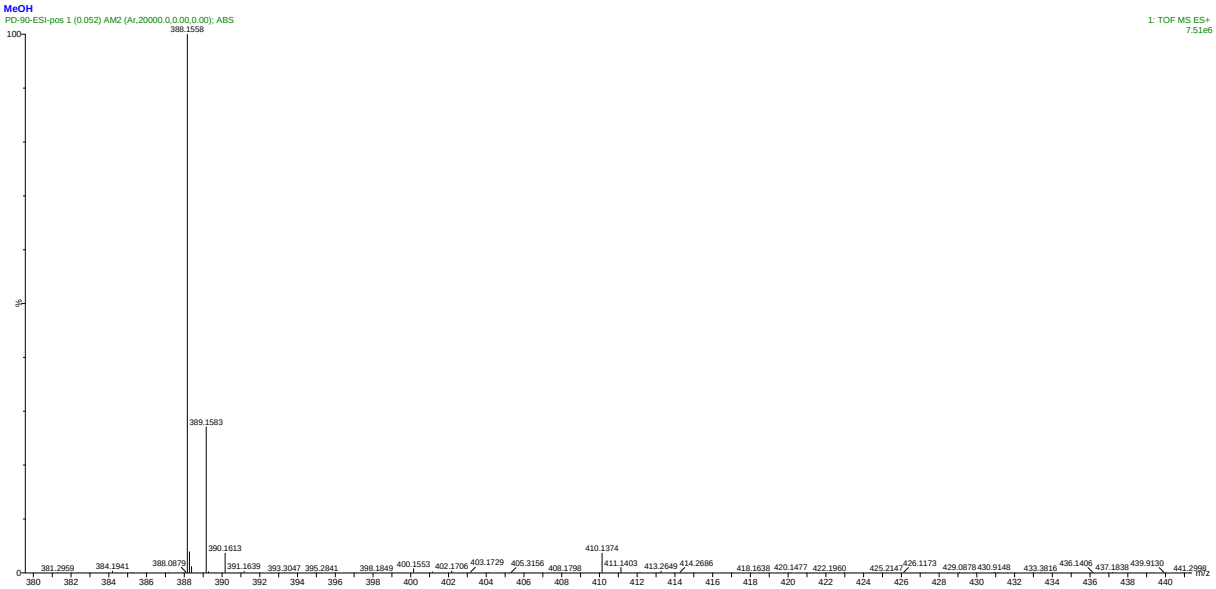

*Figure S 9: ESI-MS of 4-(anthracen-9-yl)-2,6-di(1*H*-imidazol-1-yl)pyridine **3-1** in MeOH.*

2,6-di(1*H*-imidazol-1-yl)-4-(pyren-1-yl)pyridine **3-2**:

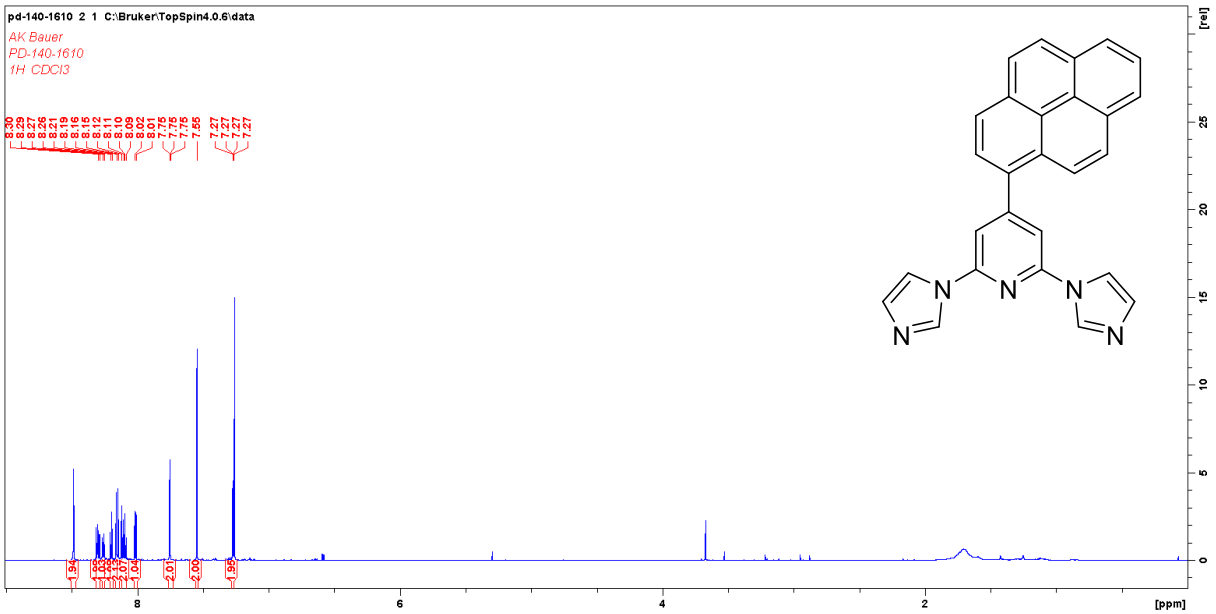

*Figure S 10: ^{1}H-NMR of 2,6-di(1*H*-imidazol-1-yl)-4-(pyren-1-yl)pyridine **3-2** in $CDCl_3$.*

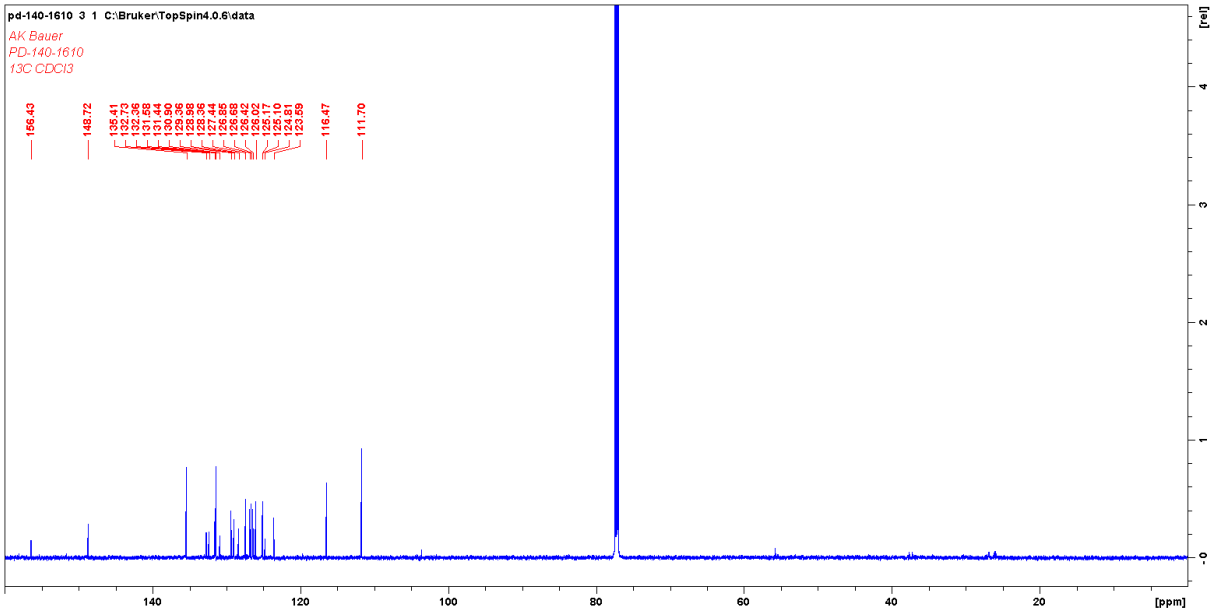

*Figure S 11: ^{13}C-NMR of 2,6-di(1H-imidazol-1-yl)-4-(pyren-1-yl)pyridine **3-2** in $CDCl_3$.*

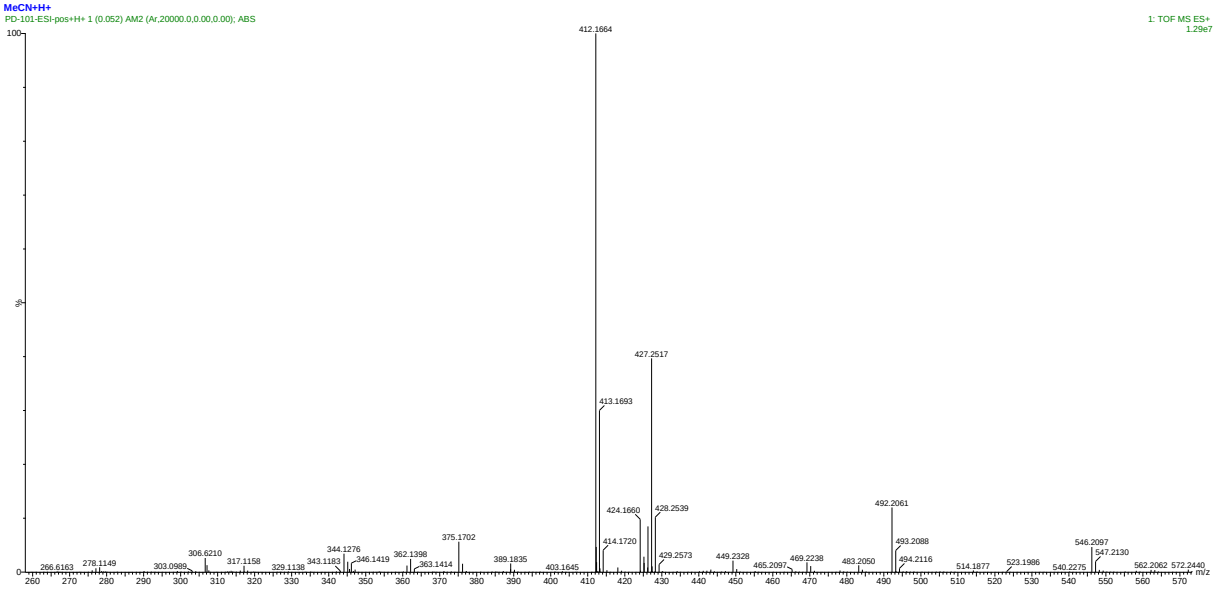

*Figure S 12: ESI-MS of 2,6-di(1H-imidazol-1-yl)-4-(pyren-1-yl)pyridine **3-2** in MeCN.*

1,1‘-(4-(anthracen-9-yl)pyridine-2,6-diyl)bis(3-methyl-1*H*-imidazol-3-ium) **[H_2-L1](PF_6)$_2$**:

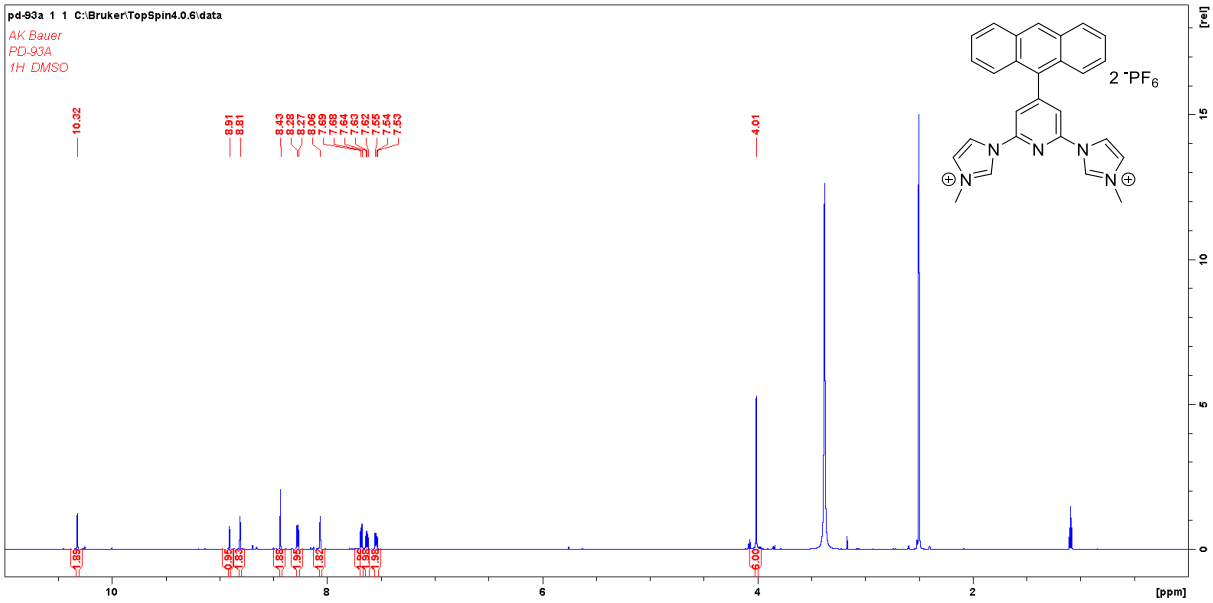

*Figure S 13: ^{1}H-NMR of 1,1‘-(4-(anthracen-9-yl)pyridine-2,6-diyl)bis(3-methyl-1*H*-imidazol-3-ium)* ***[H_2-L1](PF_6)$_2$*** *d_6-DMSO.*

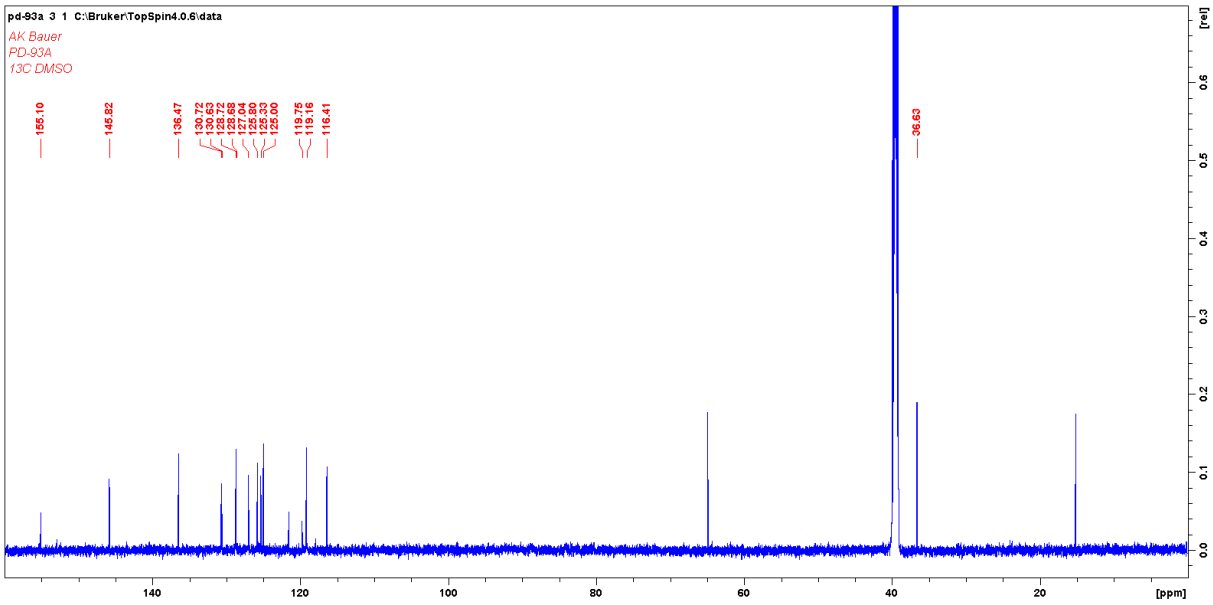

*Figure S 14: ^{13}C-NMR of 1,1‘-(4-(anthracen-9-yl)pyridine-2,6-diyl)bis(3-methyl-1*H*-imidazol-3-ium)* ***[H_2-L1](PF_6)$_2$*** *d_6-DMSO.*

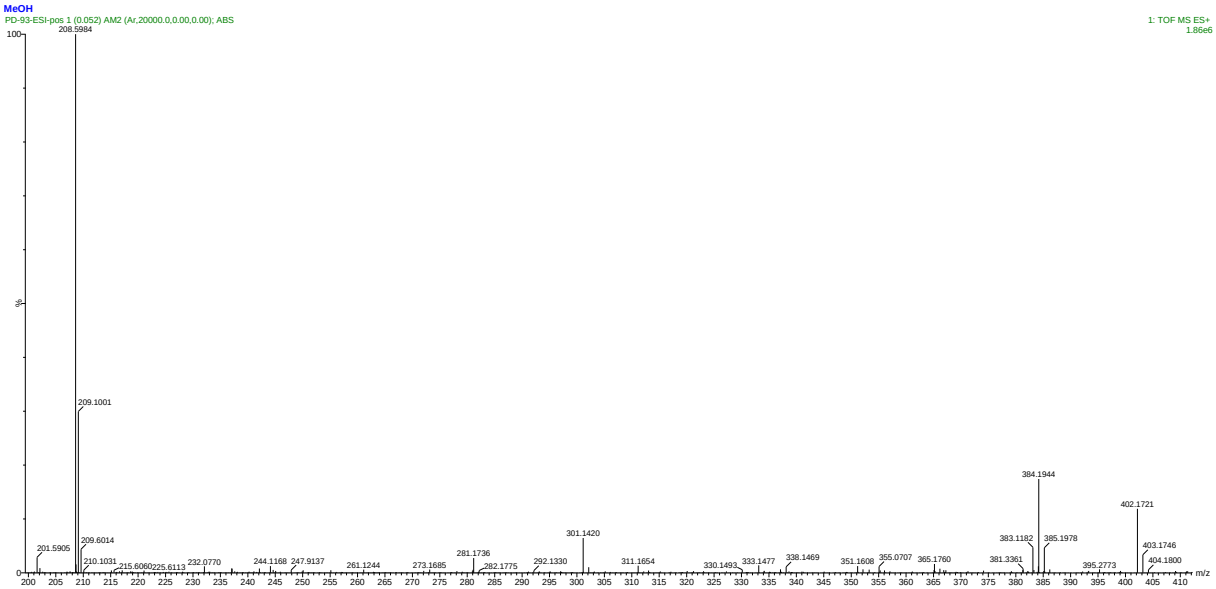

*Figure S 15: ESI-MS of 1,1'-(4-(anthracen-9-yl)pyridine-2,6-diyl)bis(3-methyl-1*H*-imidazol-3-ium)* ***[H$_2$-L1](PF$_6$)$_2$*** *in MeOH.*

1,1'-(4-(pyren-1-yl)pyridine-2,6-diyl)bis(3-methyl-1*H*-imidazol-3-ium) **[H$_2$-L2](PF$_6$)$_2$**:

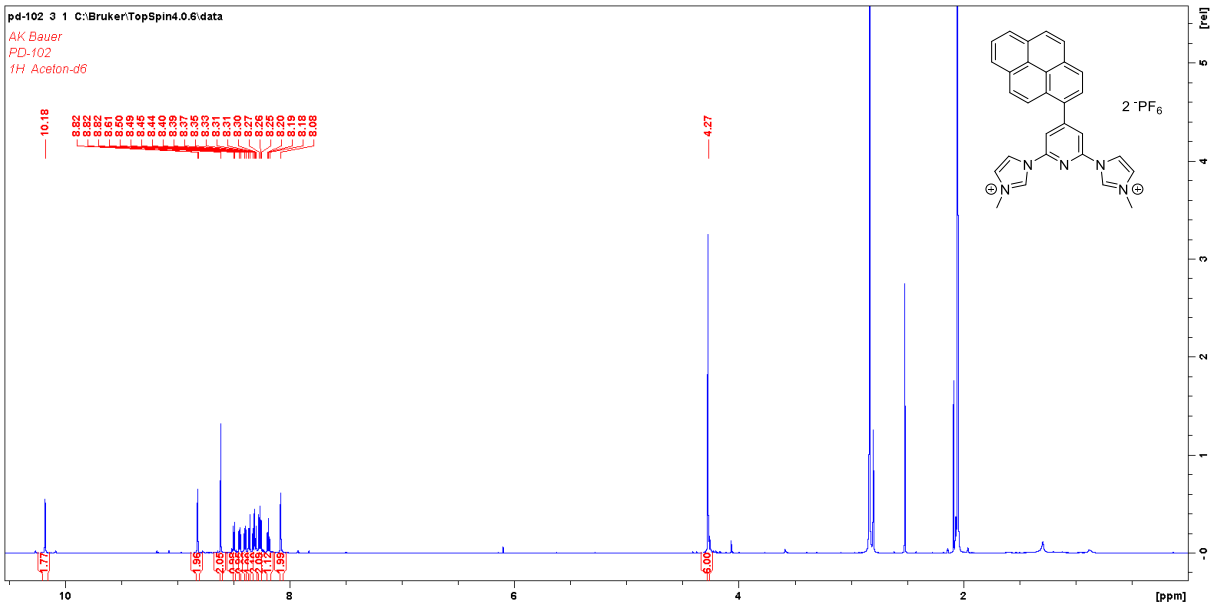

*Figure S 16: ^{1}H-NMR of 1,1'-(4-(pyren-1-yl)pyridine-2,6-diyl)bis(3-methyl-1*H*-imidazol-3-ium)* ***[H$_2$-L2](PF$_6$)$_2$*** *in d$_6$-acetone.*

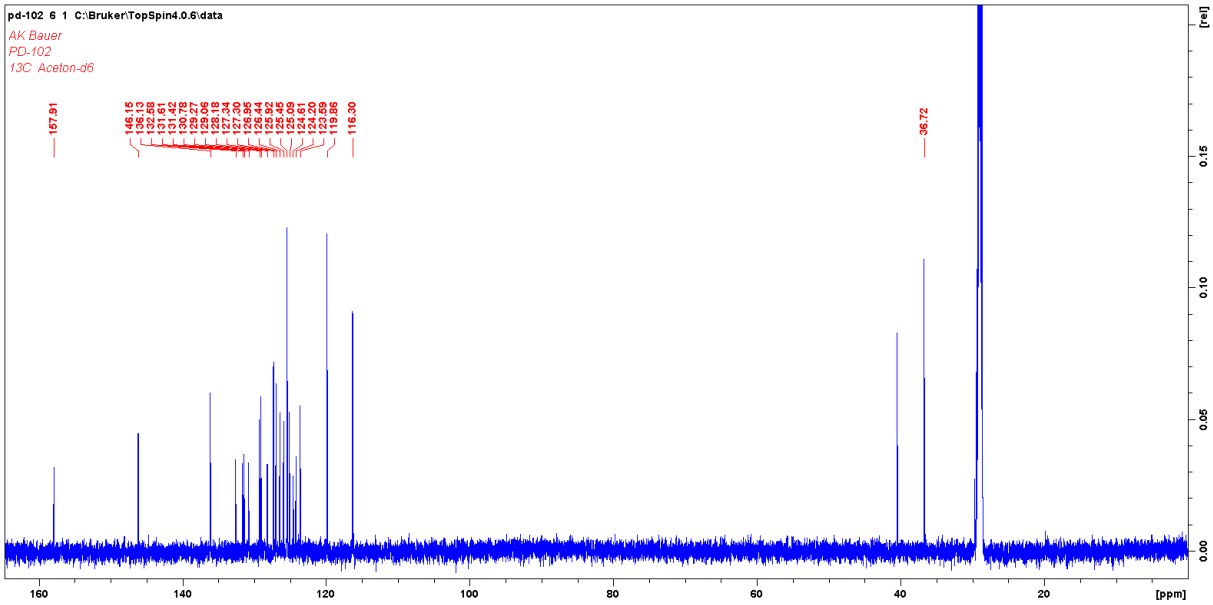

*Figure S 17: ^{13}C-NMR of 1,1'-(4-(pyren-1-yl)pyridine-2,6-diyl)bis(3-methyl-1*H*-imidazol-3-ium)* ***[H$_2$-L2](PF$_6$)$_2$*** *in d$_6$-acetone.*

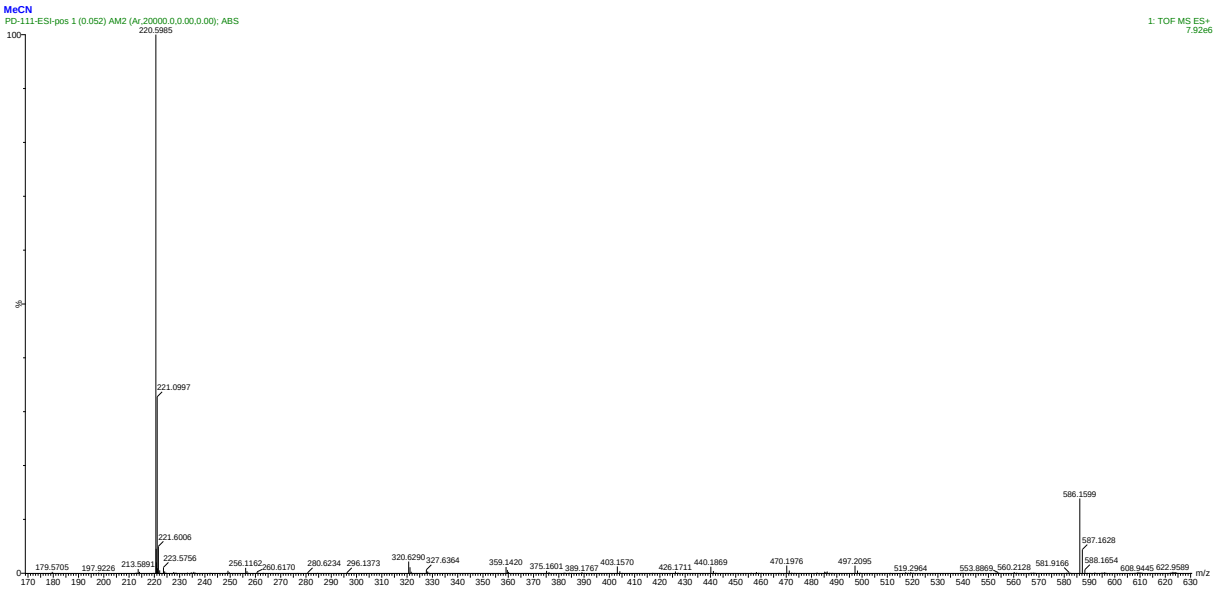

*Figure S 18: ESI-MS of 1,1'-(4-(pyren-1-yl)pyridine-2,6-diyl)bis(3-methyl-1*H*-imidazol-3-ium)* ***[H$_2$-L2](PF$_6$)$_2$*** *in MeCN.*

[Fe(bim-ant)$_2$](PF$_6$)$_2$ **[C1](PF$_6$)$_2$**:

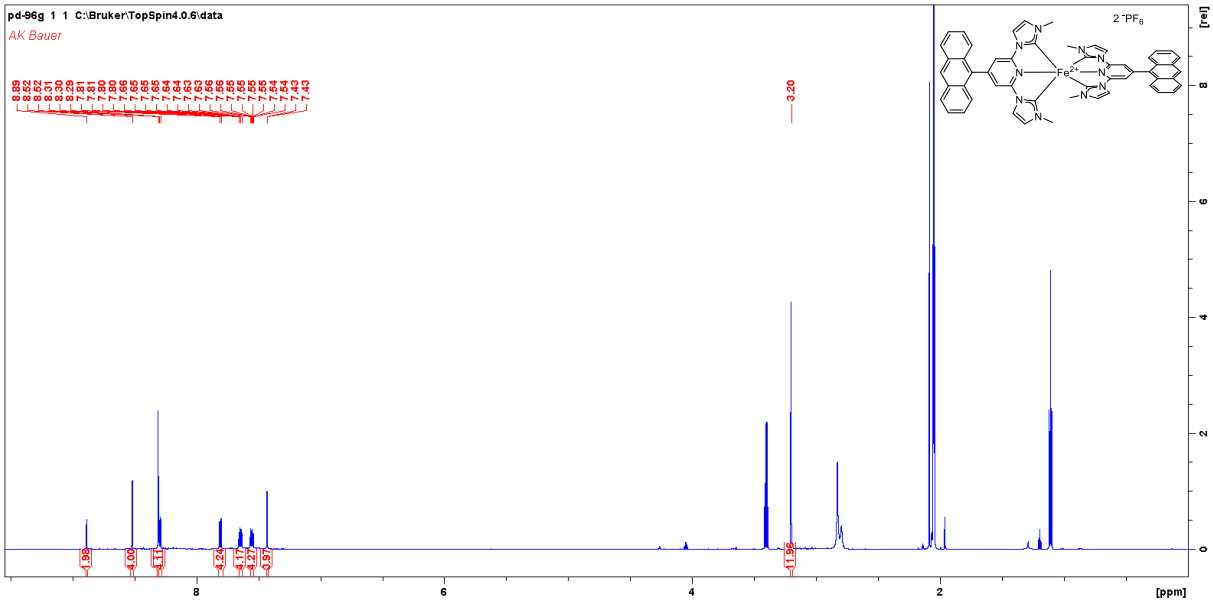

*Figure S 19: ^{1}H-NMR of [Fe(bim-ant)$_2$](PF$_6$)$_2$ **[C1](PF$_6$)$_2$** in d$_6$-acetone.*

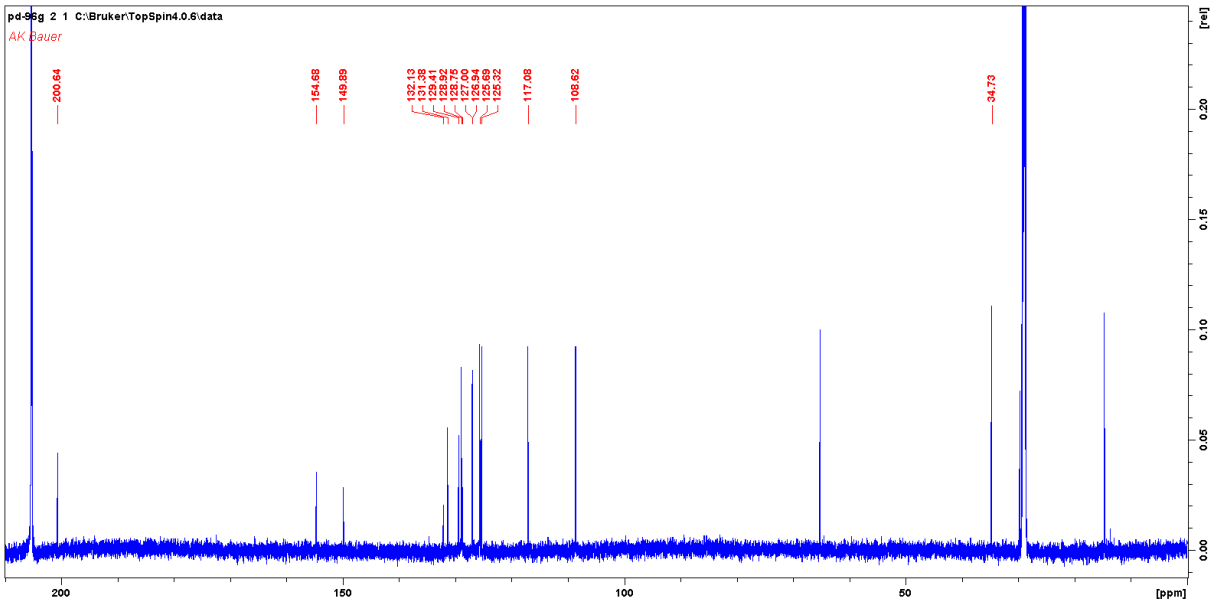

*Figure S 20: ^{31}C-NMR of [Fe(bim-ant)$_2$](PF$_6$)$_2$ **[C1](PF$_6$)$_2$** in d$_6$-acetone.*

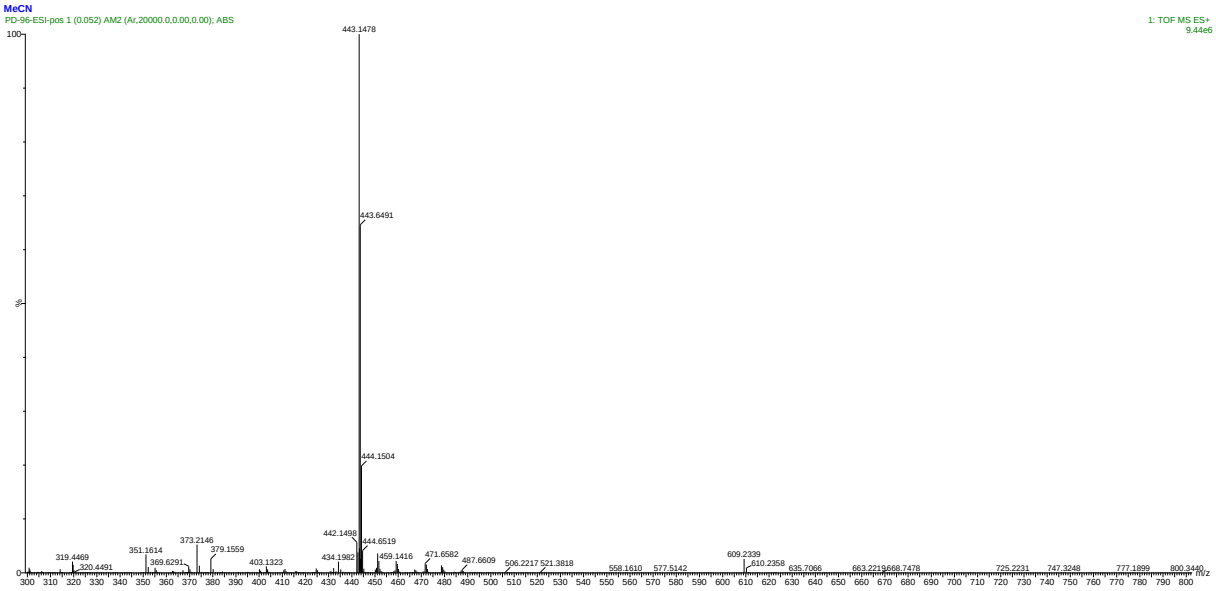

*Figure S 21: ESI-MS of $[Fe(bim\text{-}ant)_2](PF_6)_2$ **[C1](PF_6)$_2$** in MeCN.*

$[Fe(bim\text{-}pyr)_2](PF_6)_2$ **[C2](PF_6)$_2$**:

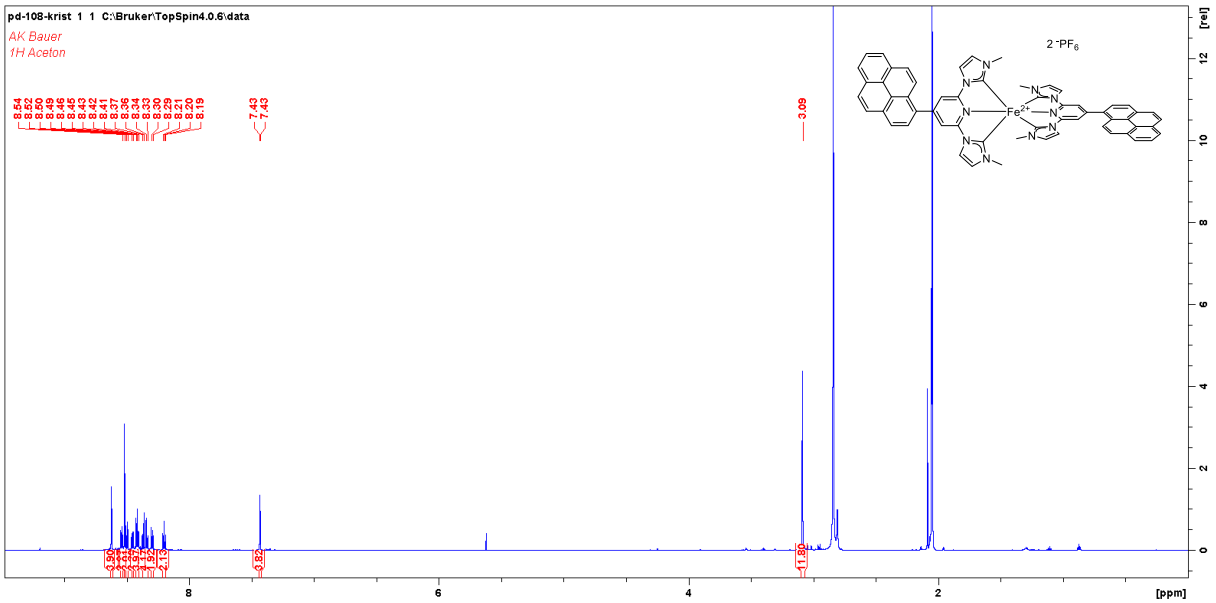

*Figure S 22: ^{1}H-NMR of $[Fe(bim\text{-}pyr)_2](PF_6)_2$ **[C2](PF_6)$_2$** d_6-acetone.*

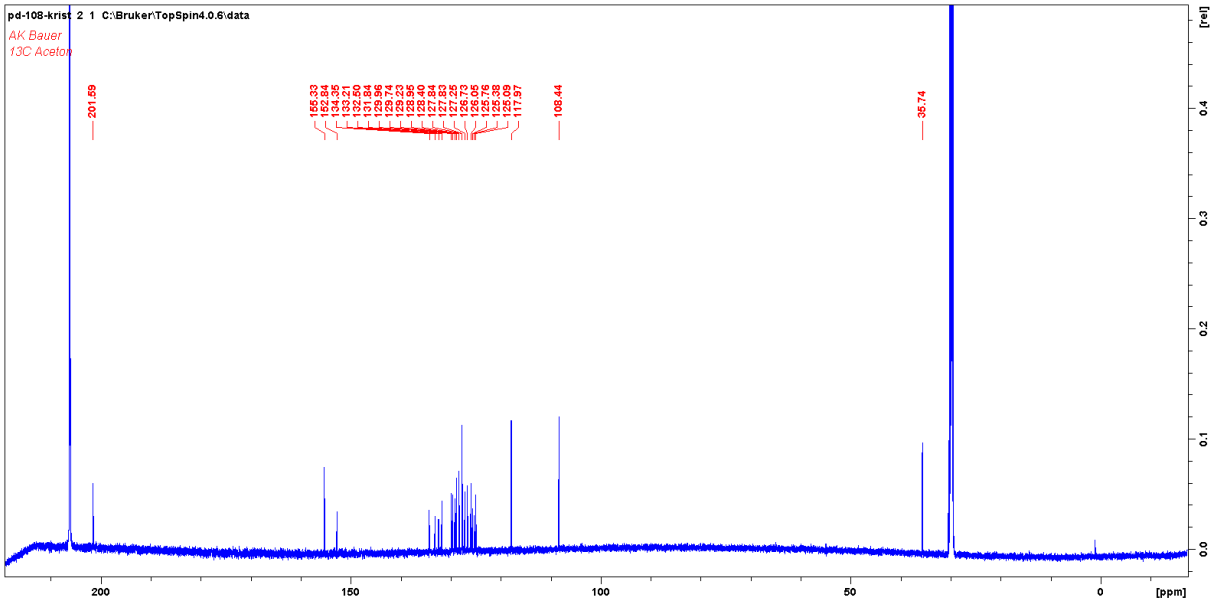

*Figure S 23: ^{13}C-NMR of [Fe(bim-pyr)$_2$](PF$_6$)$_2$ **[C2](PF$_6$)$_2$** in d$_6$-acetone.*

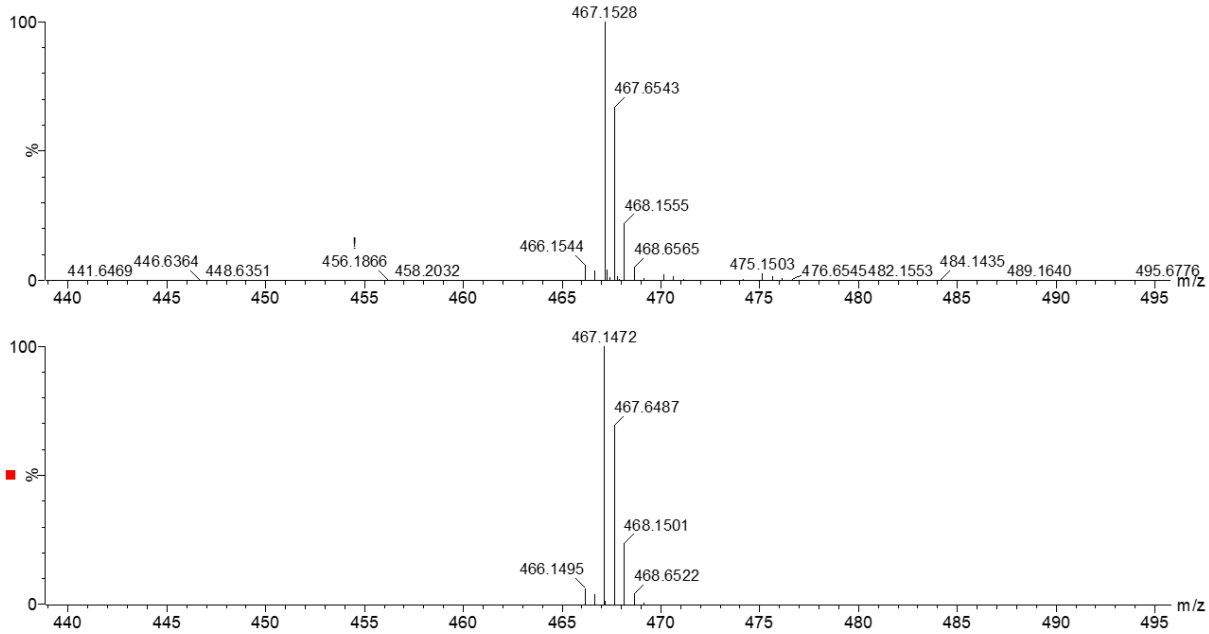

*Figure S 24: Observed isotope pattern for [Fe(bim-pyr)$_2$](PF$_6$)$_2$ **[C2](PF$_6$)$_2$** in MeCN (top) and calculated isotope pattern for $C_{58}H_{42}FeN_{10}^{2+}$ (bottom). Intensities are given in relation to the most intensive signal.*

Computational Chemistry

Table S 1: Optimal range-separation parameters for LC-BLYP calculations as obtained using the protocol described in literature.[1]

compound	α	ω, Bohr^{-1}
[C0]$^{2+}$	0.00	0.15
anthracene	0.50	0.12
pyrene	0.40	0.15

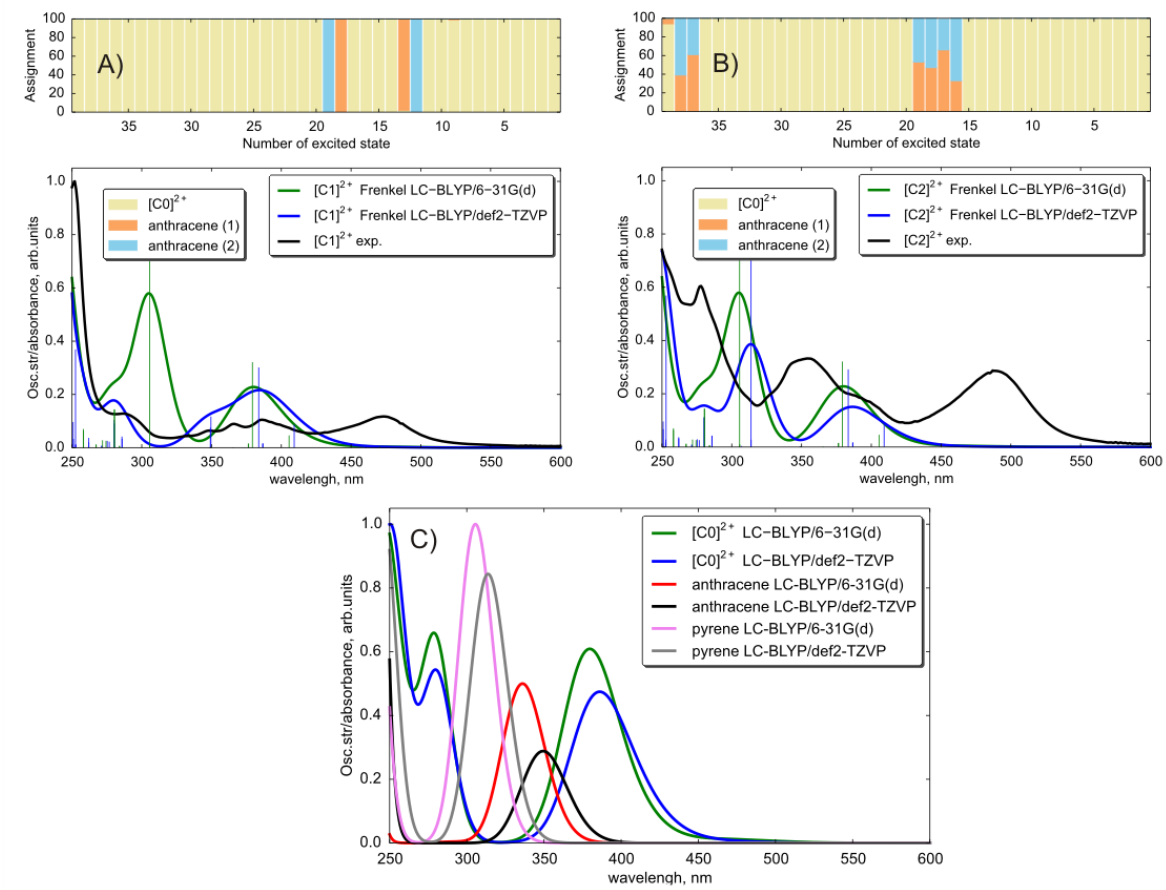

*Figure S 25: Absorption spectra of **[C1]$^{2+}$** (panel A) and **[C2]$^{2+}$** (panel B) modeled with Frenkel exciton approach compared with experiment. The spectra of **[C0]$^{2+}$**, anthracene, and pyrene computed with LC-BLYP/def2-TZVP and LC-BLYP/6-31G(d) are shown in panel C. The assignment in the upper parts of panels A) and B) corresponds to the larger basis set.*

*Table S 2: Assignment of absorption spectrum of **[C0]²⁺**.*

LC-BLYP/6-31G(d)									LC-BLYP/def2-TZVP								
state number	E, ev	wavelength, nm	osc.str.	% MC	% LC	% MLCT	% LMCT	% LLCT	state number	E, ev	wavelength, nm	osc.str.	% MC	% LC	% MLCT	% LMCT	% LLCT
1	2,634	470,711	0,003	6,4	20,1	55,1	3,9	14,6	1	2,691	460,74	0,002	5,9	21,3	53,8	3,9	15,2
2	2,635	470,532	0,003	6,4	20,1	55,1	3,9	14,6	2	2,692	460,569	0,002	5,9	21,3	53,8	3,9	15,2
3	2,867	432,456	0	7,6	7,1	68,2	2,4	14,6	3	2,848	435,341	0	7,1	7,9	67,2	2,5	15,3
4	2,924	424,026	0	10,2	7,1	64,8	3,9	14	4	2,911	425,92	0	8,9	7,9	64,7	3,5	14,9
5	3,057	405,578	0,04	4,7	18,1	65,5	1,6	10,2	5	3,031	409,057	0,072	5,1	18,5	64,7	1,9	9,7
6	3,074	403,335	0	6,9	18,3	60,3	3,4	11,1	6	3,05	406,509	0	6,3	19,4	59	3,4	11,9
7	3,272	378,928	0,283	2,7	18,9	63,5	1	14	7	3,205	386,849	0,017	6,8	18,3	64	2,6	8,3
8	3,292	376,626	0,015	9,6	16,9	62,9	3,4	7,3	8	3,207	386,608	0,017	6,6	18,5	64,1	2,5	8,3
9	3,295	376,283	0,016	9,3	17,1	63,2	3,2	7,2	9	3,236	383,143	0,253	1,6	20,6	61,4	0,7	15,8
10	3,393	365,415	0,001	5,6	8,4	69,5	1,8	14,7	10	3,32	373,449	0,001	3,5	9	70,2	1,2	16,1
11	3,394	365,307	0,001	5,7	8,4	69,4	1,8	14,6	11	3,321	373,337	0,001	3,5	9,1	70,2	1,2	16,1
12	3,546	349,648	0,003	43,5	5,3	31,3	14,1	5,9	12	3,554	348,861	0,002	45,1	5,2	28,4	15,8	5,5
13	3,547	349,549	0,003	43,2	5,3	31,6	14	5,9	13	3,554	348,861	0,002	45,1	5,2	28,4	15,8	5,5
14	3,727	332,668	0	3,3	18,1	61,5	2,4	14,7	14	3,651	339,592	0	3,1	19	60,4	2,2	15,2
15	3,798	326,449	0	37,3	7,1	23,6	24,4	7,6	15	3,876	319,879	0	35,2	8,1	23,8	24,6	8,4
16	4,209	294,572	0	36,6	8	27,8	20	7,7	16	4,293	288,808	0	36,5	8,2	26,3	21,2	7,9
17	4,365	284,044	0,007	1	51,1	15,4	7,9	24,6	17	4,338	285,812	0,043	0,5	59,1	6,4	8,5	25,5
18	4,365	284,044	0,006	1,1	50,6	16,1	7,8	24,5	18	4,339	285,746	0,043	0,5	59	6,7	8,4	25,4
19	4,421	280,446	0,148	3,2	31,4	40,7	4,5	20,2	19	4,423	280,319	0,116	0,3	28,4	51,7	1,1	18,5
20	4,423	280,319	0,144	3,4	30,3	42,1	4,4	19,8	20	4,426	280,129	0,113	0,3	28,2	52	1	18,5
21	4,519	274,364	0,023	0,3	71	5,8	9,2	13,7	21	4,48	276,753	0,022	0,2	67,6	9,7	8,2	14,3
22	4,546	272,735	0	3,7	23,3	61,9	2,2	8,9	22	4,495	275,829	0	0,2	22,9	66,1	0,5	10,3
23	4,56	271,897	0,025	4,1	22,5	62,1	2,2	9,1	23	4,505	275,217	0,025	0,3	27,3	60	1,5	11
24	4,573	271,124	0	4,6	7,6	70,7	1,6	15,6	24	4,531	273,638	0	0,2	9,1	73,4	0,1	17,1
25	4,575	271,006	0	4,6	7,6	70,4	1,6	15,7	25	4,532	273,577	0	0,3	9,1	73,2	0,2	17,2

26	4,614	268,715	0	0,8	71,4	7,8	8,3	11,7	26	4,569	271,362	0,009	20,9	11,7	50	7,5	9,9
27	4,638	267,325	0,012	23,3	10,9	48,7	8	9,1	27	4,57	271,302	0,009	20,8	12	49,6	7,6	10
28	4,638	267,325	0,012	23,4	10,8	48,6	8	9,2	28	4,572	271,184	0	0,6	72,2	6,3	8,3	12,6
29	4,703	263,63	0	0,6	20,4	4	9,6	65,4	29	4,672	265,379	0	0,8	22,2	4,4	9	63,7
30	4,737	261,738	0	0,5	19,3	4,2	9,6	66,4	30	4,7	263,798	0	0,5	21,3	4,8	8,9	64,4
31	4,801	258,249	0,069	1,4	67,4	2,6	8,1	20,6	31	4,732	262,014	0,036	1,1	67,4	2,3	7,5	21,7
32	4,801	258,249	0,07	1,4	67,4	2,5	8,2	20,6	32	4,732	262,014	0,036	1,1	67,3	2,3	7,5	21,8
33	4,973	249,317	0,005	19,2	16,7	39,2	10,4	14,4	33	4,907	252,67	0,015	21	19,3	32	11,7	16
34	4,974	249,267	0,005	19,5	16,5	39,3	10,4	14,3	34	4,909	252,567	0,015	21,2	19,3	31,9	11,7	15,9
35	5,009	247,525	0,275	0,4	47	5	9,6	38	35	4,911	252,464	0,345	0,1	49,3	6,7	8,6	35,3
36	5,012	247,377	0,005	4	35,5	19,4	4	37	36	4,925	251,747	0	4,1	41,1	16,9	3,5	34,3
37	5,024	246,786	0,081	5,4	56,6	13,5	7,5	17	37	4,933	251,338	0	9,7	18,1	47,2	7	18
38	5,025	246,737	0,081	5,4	56,6	13,4	7,5	17,1	38	4,943	250,83	0,093	8	49,3	16,7	8,1	17,8
39	5,145	240,982	0	5,2	37,4	30,6	5,9	20,9	39	4,944	250,779	0,094	7,8	49,5	16,5	8	18,1
40	5,187	239,031	0,008	0,2	18,8	4,1	4,8	72,2	40	5,05	245,515	0	6	36,5	31	7,1	19,3

*Table S 3: Assignment of absorption spectra of **[C1]$^{2+}$** and **[C2]$^{2+}$** computed with LC-BLYP/6-31G(d).*

[C1]$^{2+}$									**[C2]$^{2+}$**								
state number	E, ev	wavelength, nm	osc.str.	% MC	% LC	% MLCT	% LMCT	% LLCT	state number	E, ev	wavelength, nm	osc.str.	% MC	% LC	% MLCT	% LMCT	% LLCT
1	2,604	476,134	0,002	6,3	20,4	54,8	3,8	14,7	1	2,577	481,122	0,002	6	20,7	54,8	3,7	14,8
2	2,609	475,221	0,002	6,3	20,4	54,8	3,9	14,6	2	2,586	479,448	0,002	6,2	20,6	54,7	3,8	14,7
3	2,839	436,721	0,001	7,5	7,2	67,8	2,5	15	3	2,802	442,488	0,006	7,3	7,3	67,4	2,5	15,5
4	2,898	427,83	0	9,9	7,1	64,6	3,8	14,5	4	2,863	433,06	0	9,4	7,2	64,6	3,6	15,1
5	2,973	417,037	0,456	4,7	33,6	52,3	2,4	7	5	2,896	428,126	1,016	5,1	32,1	53,4	2,8	6,7
6	3,027	409,598	0,001	6,3	24,1	55,8	3,5	10,4	6	2,995	413,974	0	6,2	24,6	55,7	3,5	10
7	3,116	397,899	0,465	0	53,3	35,9	0,9	10	7	3,146	394,104	0,677	0	31,4	53,4	0,5	14,7
8	3,173	390,751	0,01	0,4	90,2	5,4	2	1,9	8	3,228	384,093	0,015	7,4	20,6	62	2,9	7,1
9	3,245	382,081	0,015	7,4	19,7	63	2,8	7,2	9	3,234	383,38	0,013	6,3	21,5	62,7	2,5	7,1
10	3,248	381,728	0,013	7,1	19,6	63,5	2,7	7,2	10	3,318	373,674	0,005	0,7	82,8	9,6	3,3	3,6
11	3,285	377,428	0,028	2,3	50,3	38,3	1,3	7,8	11	3,343	370,88	0,001	5,7	8,1	68,6	1,9	15,8
12	3,351	369,995	0	5,7	7,9	69	1,9	15,5	12	3,345	370,658	0	5,6	7,9	68,6	1,8	16,1
13	3,354	369,664	0,001	5,4	8	69,4	1,8	15,4	13	3,426	361,895	0,292	1,7	70,5	20,8	2,8	4,2
14	3,446	359,795	0,011	0,1	90,7	0,9	5,7	2,6	14	3,531	351,133	0,002	45,4	5,2	28,7	15,2	5,5
15	3,463	358,028	0,017	0,1	90,5	1,3	5,5	2,5	15	3,537	350,538	0,003	43,8	5,9	29,6	14,8	5,8
16	3,539	350,34	0,002	44,8	5,4	29,5	14,8	5,6	16	3,653	339,406	0	0,8	76,3	17,3	1,2	4,4
17	3,542	350,043	0,002	45	5,3	29,4	14,8	5,5	17	3,669	337,926	0,036	0,3	96,7	1,8	0,7	0,5
18	3,69	336,003	0	3,2	19,8	60,2	2,4	14,4	18	3,702	334,914	0,001	2,1	46,1	40,2	1,7	9,9
19	3,768	329,048	0,001	0,1	96,8	1,2	1,5	0,4	19	3,8	326,277	0	37,1	7,2	23,3	24,4	7,9
20	3,773	328,612	0,001	0,1	96,4	1,6	1,4	0,5	20	3,971	312,227	0,046	0,1	88,9	5,6	3,3	2,2
21	3,8	326,277	0	37,3	7,1	23,3	24,5	7,8	21	3,972	312,148	0,066	0,1	88,7	5,7	3,3	2,2
22	3,926	315,805	0,012	0,1	81,5	13,4	1	4	22	4,091	303,068	0,049	1,7	25,7	54,9	1,2	16,5
23	3,931	315,404	0,01	0,1	77,6	16,6	0,9	4,8	23	4,113	301,447	0,044	1,8	26,1	54,6	1,2	16,3

24	3,955	313,49	0,003	0,2	47,6	40,1	0,4	11,7	24	4,161	297,97	0,011	0,5	85,3	8,8	2,7	2,6
25	3,96	313,094	0,005	0,1	51,4	37,1	0,4	10,9	25	4,162	297,898	0,004	0,5	85,2	8,9	2,7	2,7
26	4,117	301,154	0,003	0,3	26,9	65	0,1	7,7	26	4,207	294,712	0	35,9	8,1	28,3	19,8	7,9
27	4,118	301,081	0	0,3	26,7	65	0,1	7,8	27	4,26	291,045	0,195	1,8	44,3	39,5	2,9	11,5
28	4,203	294,992	0	36	8,1	28,2	19,9	7,9	28	4,262	290,908	0,024	1,8	43	42,1	2,6	10,6
29	4,306	287,936	0,017	0,7	57,4	9,3	8,1	24,5	29	4,283	289,482	0,046	0,8	59	15,7	5,9	18,7
30	4,315	287,335	0,016	0,7	57,1	9,4	8,2	24,6	30	4,287	289,212	0,033	0,7	60,4	13,3	6,4	19,2
31	4,332	286,208	0	0,9	7,7	71,1	0,3	19,9	31	4,325	286,671	0,012	2,7	10,7	66,5	1,1	19
32	4,34	285,68	0	0,7	7,7	70,9	0,3	20,4	32	4,333	286,142	0	3	8,7	68,1	1,2	18,9
33	4,388	282,555	0,086	3,3	28,2	46,5	3,5	18,5	33	4,346	285,286	0,003	0,1	94,6	2	1,5	1,8
34	4,404	281,529	0,104	3,4	27,1	48,2	3,4	18	34	4,346	285,286	0,003	0,1	94,6	1,9	1,5	1,8
35	4,47	277,372	0,033	0,2	73,7	3,3	9,2	13,6	35	4,413	280,954	0,457	0,1	92,2	4	2,1	1,6
36	4,515	274,607	0	3	28,8	55,9	2,8	9,5	36	4,417	280,7	0,012	0,1	93,3	3	2,1	1,5
37	4,531	273,638	0,036	3,8	21,2	63,9	1,9	9,2	37	4,435	279,561	0,011	0,2	75,9	2,9	8,5	12,4
38	4,535	273,396	0	0,1	5,1	1,3	8,9	84,7	38	4,445	278,932	0,043	0,1	94,7	2,6	1,5	1,2
39	4,548	272,615	0	0,1	5,1	1,6	9	84,2	39	4,445	278,932	0,044	0,1	94,9	2,5	1,5	1,1
40	4,558	272,017	0	1,2	65,7	14,3	7,3	11,4	40	4,504	275,278	0	0,3	76,2	4,1	8,2	11,1

*Table S 4: Assignment of absorption spectra of **[C1]²⁺** and **[C2]²⁺** computed with Frenkel exciton approach.*

[C1]²⁺ based on LC-BLYP/6-31G(d)						**[C1]²⁺** based on LC-BLYP/def2-TZVP					**[C2]²⁺** based on LC-BLYP/6-31G(d)					**[C2]²⁺** based on LC-BLYP/def2-TZVP				
State number	wavelength, nm	osc.str.	% $[C0]^{2+}$	% ant1	% ant2	wavelength, nm	osc.str.	% $[C0]^{2+}$	% ant1	% ant1	wavelength, nm	osc.str.	% $[C0]^{2+}$	% pyr1	% pyr1	wavelength, nm	osc.str.	% $[C0]^{2+}$	% pyr1	% pyr1
1	470,73	0,003	1	0	0	460,77	0,0021	1	0	0	470,73	0,0031	1	0	0	460,77	0,0022	1	0	0
2	470,5	0,0027	1	0	0	460,59	0,0019	1	0	0	470,5	0,0028	1	0	0	460,59	0,002	1	0	0
3	432,47	0	1	0	0	435,33	0	1	0	0	432,47	0	1	0	0	435,33	0	1	0	0
4	424,08	0	1	0	0	425,93	0	1	0	0	424,08	0	1	0	0	425,93	0	1	0	0
5	405,61	0,0473	1	0	0	409,25	0,0865	1	0	0	405,58	0,0462	1	0	0	409,18	0,084	1	0	0
6	403,36	0	1	0	0	406,54	0	1	0	0	403,36	0	1	0	0	406,54	0	1	0	0
7	379,6	0,3285	0,99	0,01	0	386,83	0,0163	1	0	0	379,3	0,3212	1	0	0	386,83	0,0176	1	0	0
8	376,59	0,0149	1	0	0	386,64	0,0158	1	0	0	376,59	0,0156	1	0	0	386,63	0,0163	1	0	0
9	376,35	0,0144	1	0	0	383,82	0,3013	0,99	0,01	0	376,34	0,0149	1	0	0	383,47	0,2916	1	0	0
10	365,43	0,0013	1	0	0	373,48	0,0005	1	0	0	365,43	0,0013	1	0	0	373,48	0,0005	1	0	0
11	365,36	0,0012	1	0	0	373,39	0,0006	1	0	0	365,36	0,0013	1	0	0	373,39	0,0006	1	0	0
12	349,64	0,0022	1	0	0	349,58	0,1171	0	0	1	349,64	0,0024	1	0	0	348,91	0,0017	1	0	0
13	349,55	0,0026	1	0	0	349,14	0,0751	0,02	0,98	0	349,55	0,0027	1	0	0	348,86	0,0019	1	0	0
14	336,19	0,134	0	0	1	348,91	0,0015	1	0	0	332,69	0	1	0	0	339,61	0	1	0	0
15	335,87	0,0914	0,01	0,99	0	348,86	0,0019	1	0	0	326,41	0	1	0	0	319,89	0	1	0	0
16	332,69	0	1	0	0	339,61	0	1	0	0	305,75	0,0101	0	0,4	0,6	313,9	0,0276	0	0,33	0,67
17	326,41	0	1	0	0	319,89	0	1	0	0	305,63	0,9157	0	0,6	0,4	313,8	0,8957	0	0,66	0,33
18	294,56	0	1	0	0	297,75	0,0001	0	1	0	300,11	0,0001	0	0,42	0,58	307,08	0	0	0,47	0,53
19	290,43	0	0	0,59	0,41	297,75	0	0	0	1	300,1	0,0013	0	0,58	0,42	307,06	0,004	0	0,53	0,47
20	290,41	0,0013	0	0,41	0,59	288,78	0	1	0	0	294,56	0	1	0	0	288,78	0	1	0	0
21	284,06	0,0058	1	0	0	285,88	0,0336	1	0	0	284,06	0,0071	1	0	0	285,84	0,0428	1	0	0
22	284,03	0,0062	1	0	0	285,77	0,042	1	0	0	284,03	0,0061	1	0	0	285,77	0,0419	1	0	0
23	280,52	0,1124	1	0	0	280,35	0,0906	1	0	0	280,48	0,1439	1	0	0	280,32	0,1137	1	0	0
24	280,42	0,1452	1	0	0	280,2	0,1036	1	0	0	280,34	0,144	1	0	0	280,12	0,1102	1	0	0

25	274,37	0,0234	1	0	0	276,73	0,0226	1	0	0	274,38	0,0261	1	0	0	276,74	0,026	1	0	0
26	272,74	0	1	0	0	275,83	0	1	0	0	272,74	0	1	0	0	275,83	0	1	0	0
27	271,89	0,0251	1	0	0	275,25	0,0256	1	0	0	271,89	0,0281	1	0	0	275,25	0,0292	1	0	0
28	271,12	0,0001	1	0	0	273,64	0	1	0	0	271,12	0,0001	1	0	0	273,64	0	1	0	0
29	270,98	0	1	0	0	273,56	0	1	0	0	270,98	0	1	0	0	273,56	0	1	0	0
30	268,73	0	1	0	0	271,34	0,0082	1	0	0	268,73	0	1	0	0	271,34	0,0089	1	0	0
31	267,33	0,0114	1	0	0	271,31	0,0064	1	0	0	267,33	0,0122	1	0	0	271,3	0,0083	1	0	0
32	267,32	0,0095	1	0	0	271,21	0	1	0	0	267,31	0,0117	1	0	0	271,21	0,0001	1	0	0
33	263,61	0	1	0	0	265,4	0	1	0	0	263,61	0	1	0	0	265,4	0	1	0	0
34	261,75	0	1	0	0	263,78	0	1	0	0	261,75	0	1	0	0	263,78	0	1	0	0
35	258,31	0,0435	1	0	0	262,08	0,0201	1	0	0	258,25	0,064	1	0	0	262,04	0,0324	1	0	0
36	258,23	0,0711	1	0	0	262,02	0,0368	1	0	0	258,23	0,0703	1	0	0	262,02	0,0368	1	0	0
37	249,32	0,0036	1	0	0	252,7	0,0097	1	0	0	249,31	0,0049	1	0	0	261,77	0	0	0,61	0,39
38	249,27	0,0045	1	0	0	252,59	0,0136	1	0	0	249,27	0,0051	1	0	0	261,77	0	0	0,39	0,61
39	247,55	0,2896	1	0	0	252,53	0,3689	1	0	0	248,91	0	0	0,96	0,04	252,94	0,569	0,94	0,06	0
40	247,4	0,0024	1	0	0	251,76	0,0001	1	0	0	248,91	0	0	0,04	0,96	252,67	0,0282	1	0	0

Electrochemistry

Reversibility of the oxidation of the complexes between 0.3 V and 0.4 V assigned to the oxidation of Fe^{2+} to Fe^{3+} has been tested by the criterion of Nicholson[2] and the Randles-Sevcik-equation.[3]

Electrochemical data of $[C0]^{2+}$

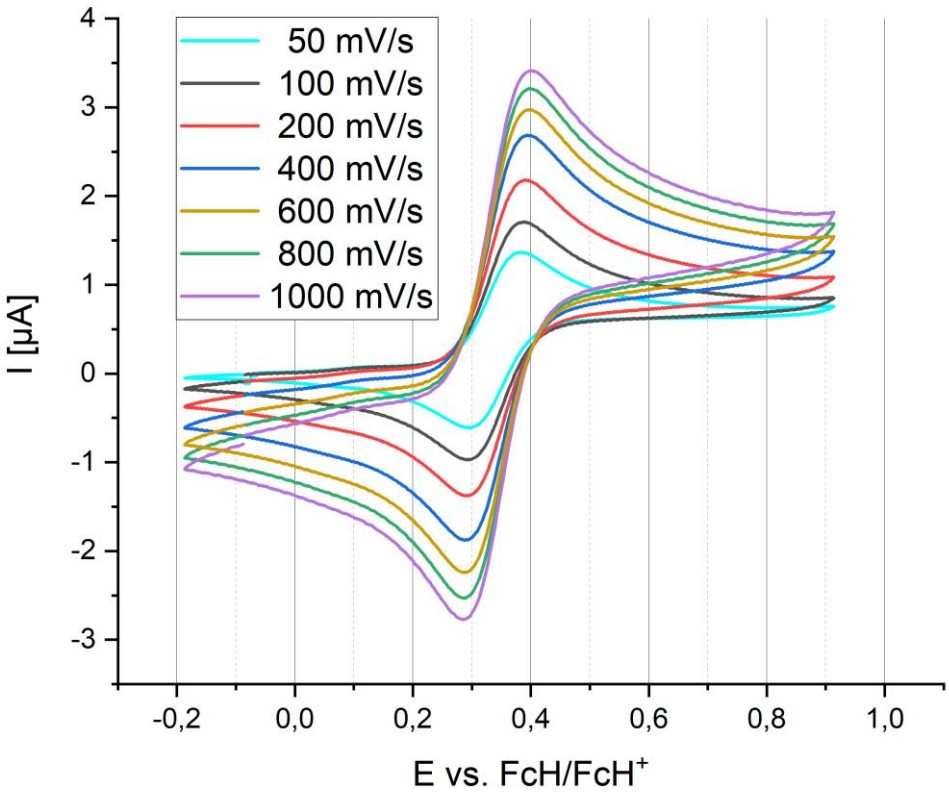

*Figure S 26: Cyclic voltammograms of the reversible oxidation of **$[C0]^{2+}$** at $E_{1/2}$ = 0.34 V vs. FcH/FcH^+ recorded at different scan rates confirming the diagnostic criterion of Nicholson.*

*Table S 5: Electrochemical data for the reversible oxidation of **$[C0]^{2+}$** at $E_{1/2}$ = 0.34 V vs. Fc/Fc^+.*

scan rate	[mV/s]	50	100	200	400	600	800	1000
E_{cat}	[V]	0.30	0.30	0.29	0.30	0.29	0.29	0.29
E_{an}	[V]	0.38	0.38	0.39	0.39	0.40	0.39	0.39
$E_{1/2}$	[V]	0.34	0.34	0.34	0.34	0.34	0.34	0.34
ΔE	[V]	0.08	0.08	0.10	0.10	0.10	0.10	0.10
I_{an}	[µA]	1.06	1.41	1.82	2.31	2.64	2.89	3.09
$\lvert I_{cat} \rvert$	[µA]	1.01	1.33	1.72	2.22	2.58	2.86	3.08
$\lvert I_{an}/I_{cat} \rvert$	[-]	1.05	1.05	1.06	1.04	1.02	1.01	1.00

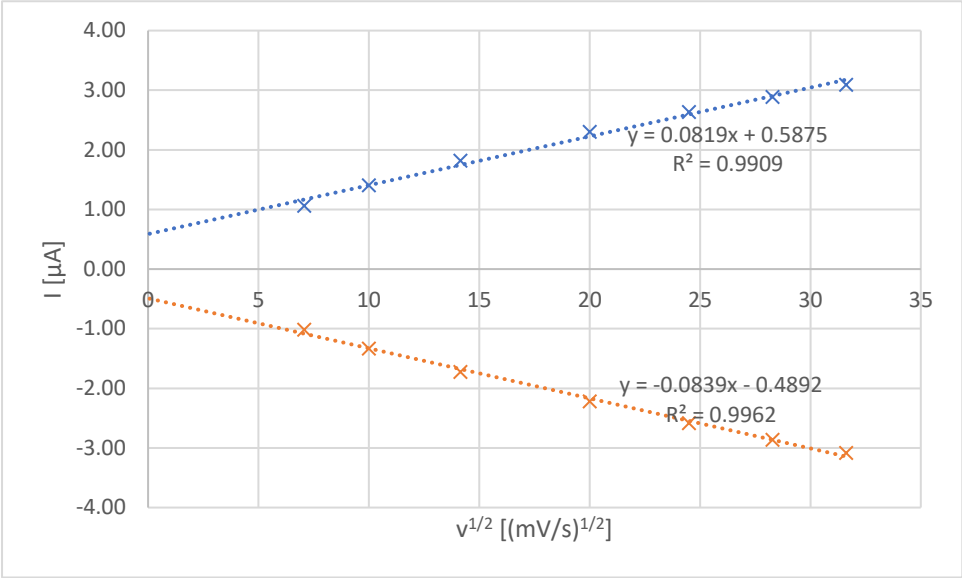

*Figure S 27: Linear dependence of forward current peaks I_{an} and I_{cat} versus the square root of the scan rate for the reversible oxidation of **[C0]**$^{2+}$ at $E_{1/2}$ = 0.34 V vs. FcH/FcH^{+}.*

Electrochemical data of [C1]$^{2+}$

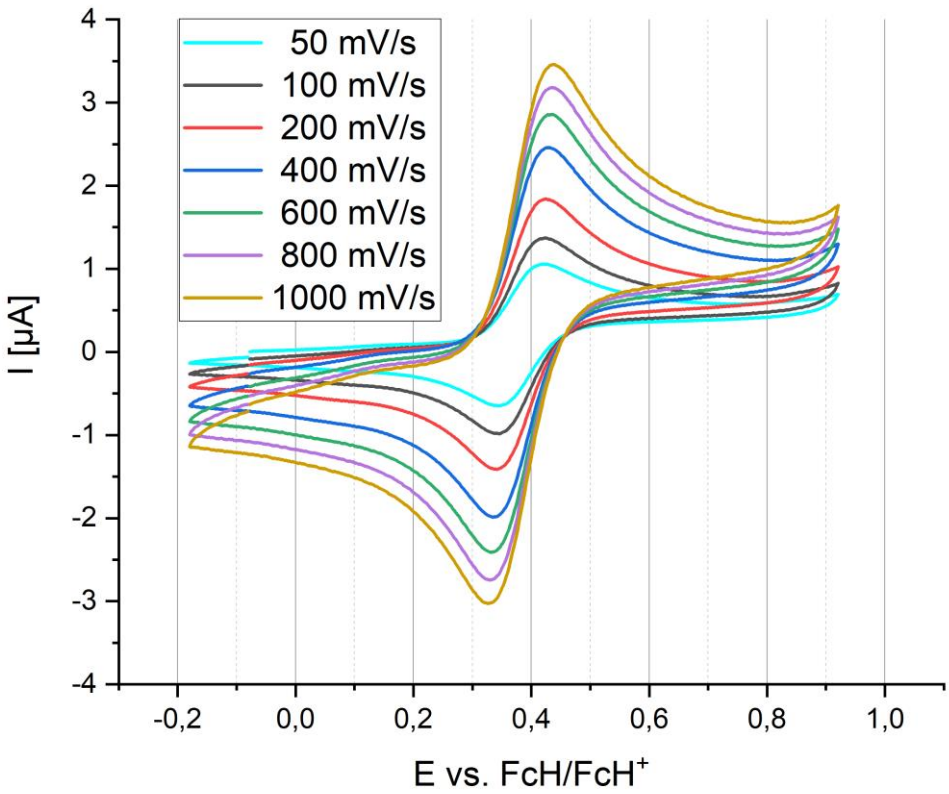

*Figure S 28: Cyclic voltammograms of the reversible oxidation of **[C1]**$^{2+}$ at $E_{1/2}$ = 0.38 V vs. FcH/FcH^{+} recorded at different scan rates confirming the diagnostic criterion of Nicholson.*

*Table S 6: Electrochemical data for the reversible oxidation of **[C1]²⁺** at $E_{1/2}$ = 0.38 V vs. FcH/FcH⁺.*

scan rate	[mV/s]	50	100	200	400	600	800	1000
E_{cat}	[V]	0.35	0.34	0.34	0.34	0.34	0.34	0.33
E_{an}	[V]	0.42	0.42	0.42	0.42	0.43	0.43	0.43
$E_{1/2}$	[V]	0.38	0.38	0.38	0.38	0.38	0.39	0.38
ΔE	[V]	0.07	0.08	0.08	0.09	0.09	0.10	0.10
I_{an}	[µA]	0.80	1.09	1.52	2.08	2.47	2.78	3.04
$\lvert I_{cat} \rvert$	[µA]	0.86	1.18	1.60	2.18	2.58	2.90	3.16
$\lvert I_{an}/I_{cat} \rvert$	[-]	0.93	1.08	1.05	1.05	1.05	1.04	1.04

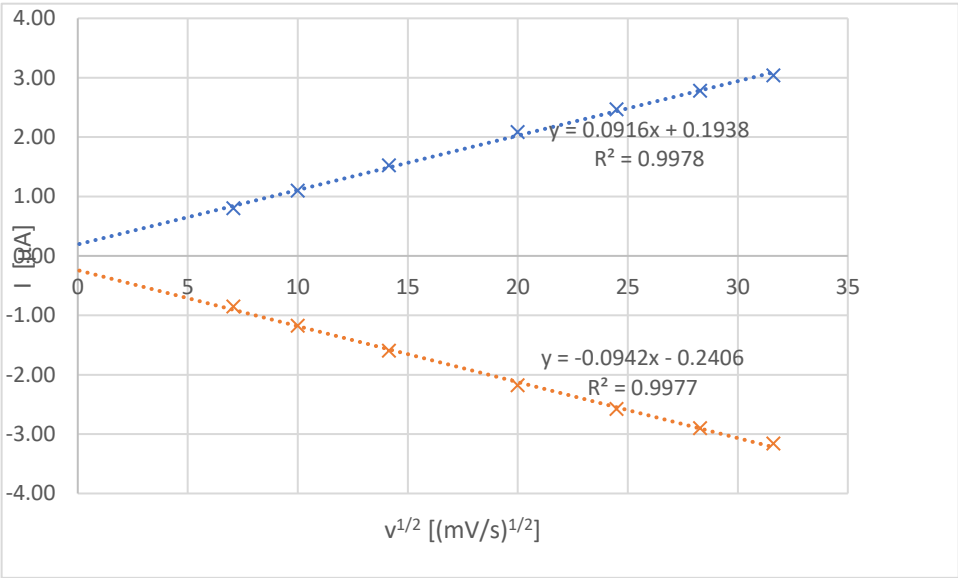

*Figure S 29: Linear dependence of forward current peaks I_{an} and I_{cat} versus the square root of the scan rate for the reversible oxidation of **[C1]²⁺** at $E_{1/2}$ = 0.38 V vs. FcH/FcH⁺.*

Electrochemical data of $[C2]^{2+}$

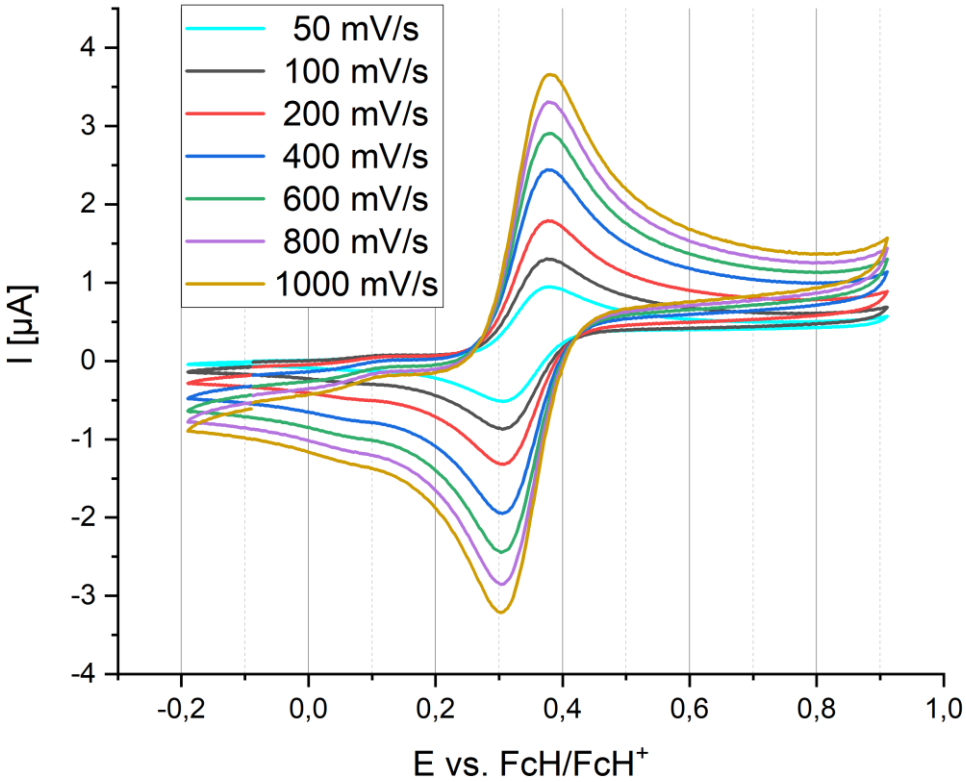

*Figure S 30: Cyclic voltammograms of the reversible oxidation of **$[C2]^{2+}$** at $E_{1/2}$ = 0.34 V vs. FcH/FcH⁺ recorded at different scan rates confirming the diagnostic criterion of Nicholson.*

*Table S 7:Electrochemical data for the reversible oxidation of **$[C2]^{2+}$** at $E_{1/2}$ = 0.34 V vs. FcH/FcH⁺.*

scan rate	[mV/s]	50	100	200	400	600	800	1000
E_{cat}	[V]	0.31	0.31	0.31	0.31	0.30	0.31	0.31
E_{an}	[V]	0.37	0.38	0.37	0.37	0.37	0.38	0.38
$E_{1/2}$	[V]	0.34	0.35	0.34	0.34	0.34	0.34	0.34
ΔE	[V]	0.06	0.07	0.07	0.07	0.07	0.07	0.08
I_{an}	[µA]	0.76	1.08	1.53	2.16	2.63	3.04	3.40
$\lvert I_{cat} \rvert$	[µA]	0.79	1.11	1.57	2.20	2.67	3.09	3.44
$\lvert I_{an}/I_{cat} \rvert$	[-]	0.96	0.97	0.98	0.98	0.99	0.98	0.99

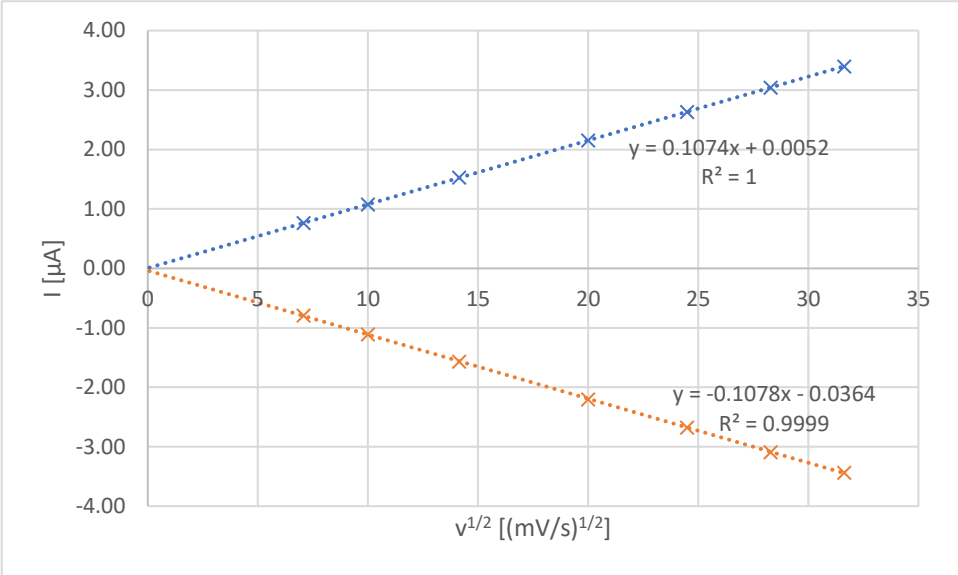

*Figure S 31: Linear dependence of forward current peaks I_{an} and I_{cat} versus the square root of the scan rate for the reversible oxidation of **[C2]**$^{2+}$ at $E_{1/2}$ = 0.34 V vs. FcH/FcH^{+}.*

Cyclic voltammetry of $[H_2\text{-}L0]^{2+}$, $[H_2\text{-}L1]^{2+}$ and $[H_2\text{-}L2]^{2+}$

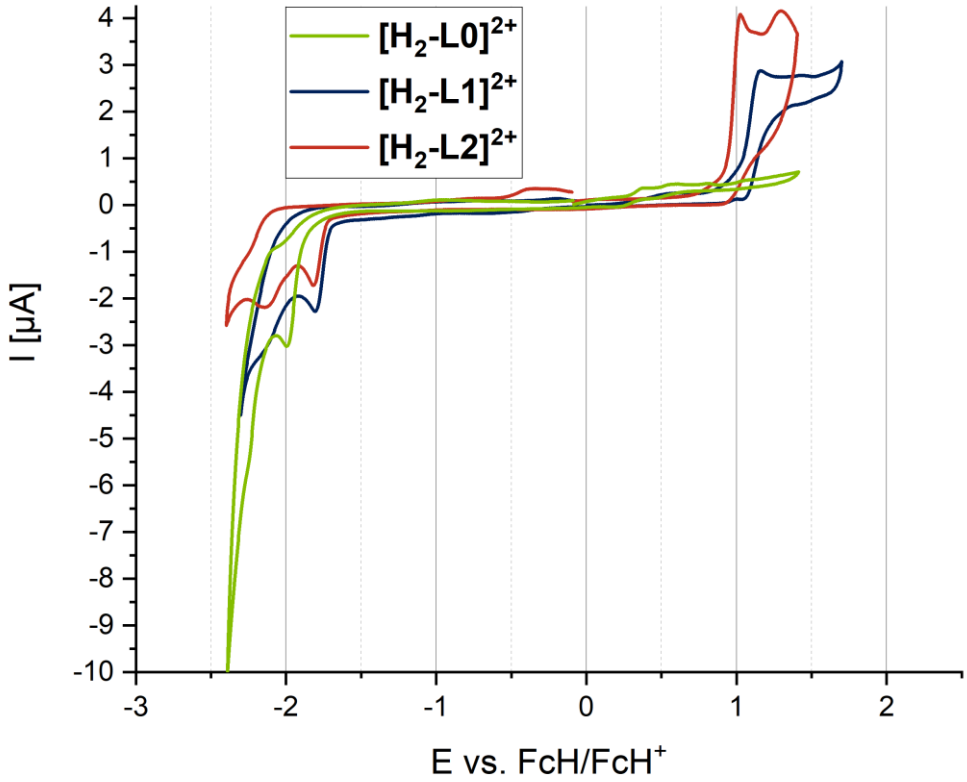

*Figure S 32: Cyclic voltammograms of Ligands **$[H_2\text{-}L0]^{2+}$-$[H_2\text{-}L2]^{2+}$** vs. FcH/FcH^+ with 100 mV/s scan rate.*

Cyclic voltammetry of **$[H_2\text{-}L0]^{2+}$** shows the first irreversible reduction peak at -2.0 V. No oxidation is observed. The first peaks of the irreversible reduction of **$[H_2\text{-}L1]^{2+}$** (-1.8 V) and **$[H_2\text{-}L2]^{2+}$** (-1.8 V) are at more anodic potentials, in line with the interpretation of **$[H_2\text{-}L1]^{2+}$** and **$[H_2\text{-}L2]^{2+}$** as better π-acceptors than **$[H_2\text{-}L0]^{2+}$**. Irreversible oxidation occurs at 1.2 V (**$[H_2\text{-}L1]^{2+}$**) and 1.0 V (**$[H_2\text{-}L2]^{2+}$**) assigned to oxidation of the organic chromophores.

Cyclic voltammetry of anthracene and pyrene

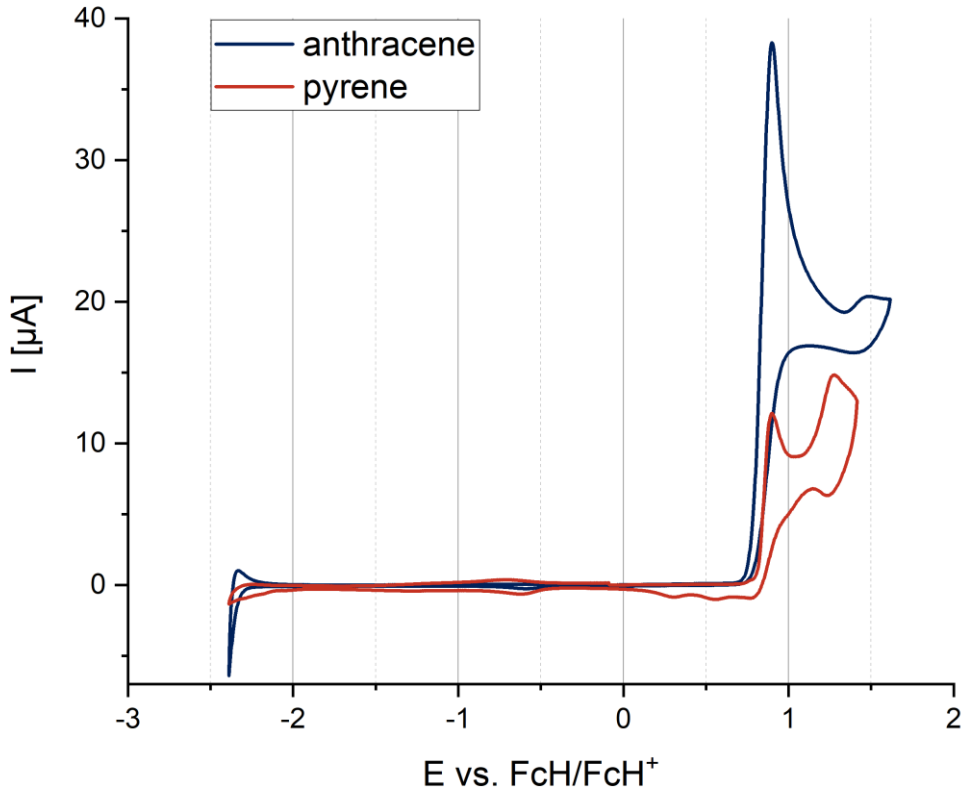

Figure S 33: Cyclic voltammograms of anthracene and pyrene vs. FcH/FcH⁺ with 100 mV/s scan rate.

Irreversible oxidation occurs at 0.9 V for both compounds, anthracene and pyrene, assigned to the oxidation of the organic chromophores, confirming the interpretation of the irreversible oxidation in **[H_2-L1]$^{2+}$**, **[H_2-L2]$^{2+}$**, **[C1]$^{2+}$** and **[C2]$^{2+}$** corresponding to the oxidation of the organic chromophores.

Spectroelectrochemistry

Spectroelectrochemical data of [C1]$^{2+}$

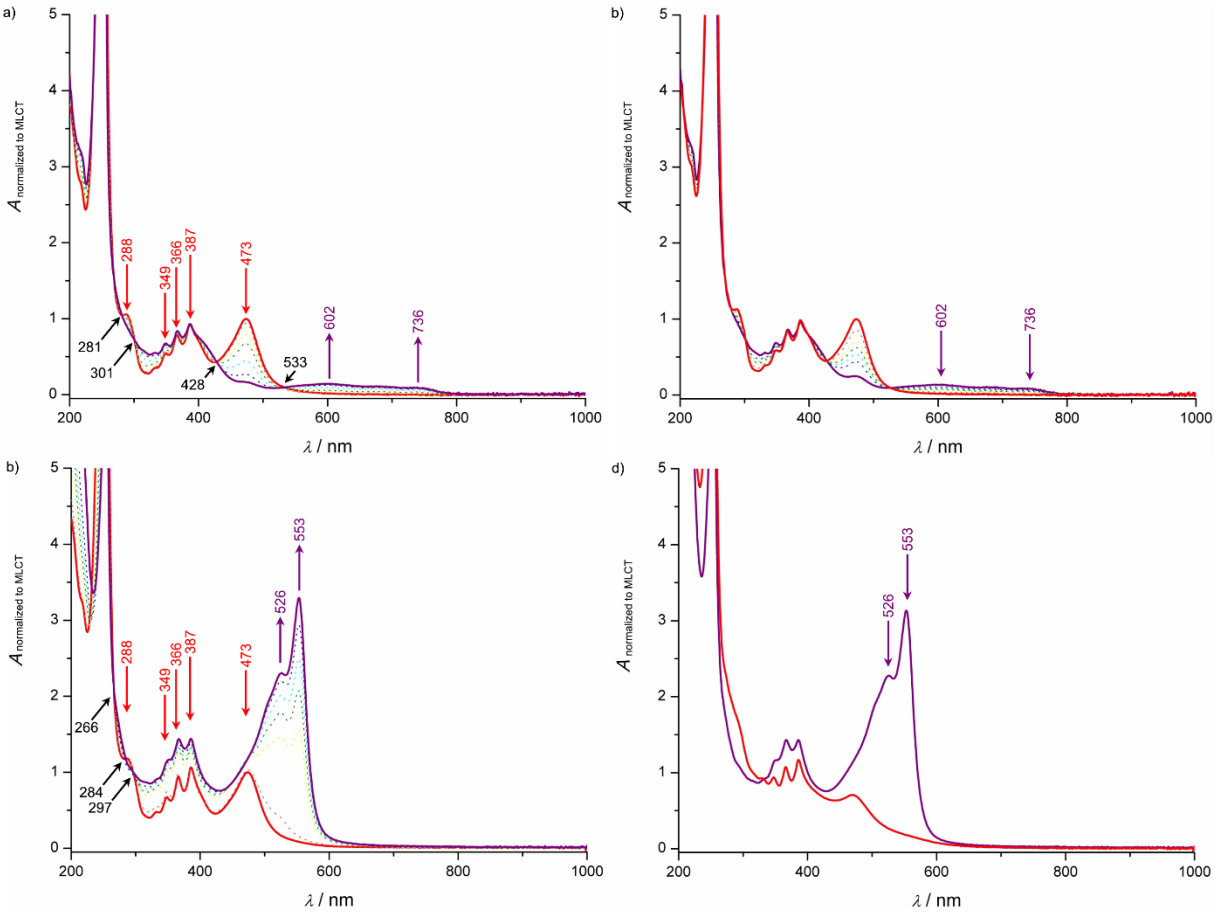

*Figure S 34: Changes in the UV/Vis/NIR spectra of **[C1]$^{2+}$** a) during oxidation (red → purple), b) during re-reduction (purple → red), c) during reduction (red → purple) and d) during re-oxidation (purple → red) in MeCN/[n-Bu$_4$N][PF$_6$].*

Spectroelectrochemical data of [C2]$^{2+}$

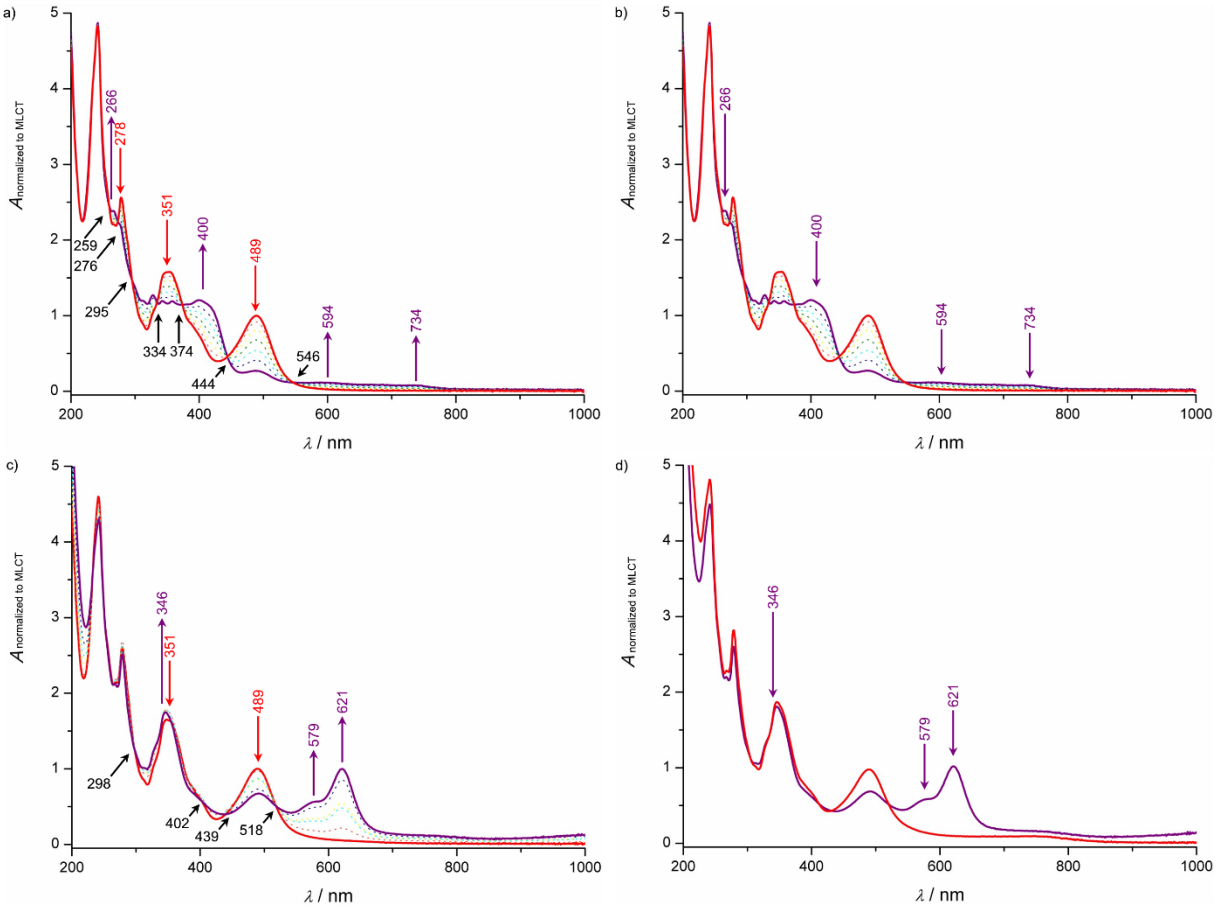

*Figure S 35: Changes in the UV/Vis/NIR spectra of **[C2]$^{2+}$** a) during oxidation (red → purple), b) during re-reduction (purple → red), c) during reduction (red → purple) and d) during re-oxidation (purple → red) in MeCN/[n-Bu$_4$N][PF$_6$].*

Ground state absorption spectra A_{gr} and absorption spectra of the oxidized states A_{ox} and reduced states A_{red} were used to approximate the excited-state differential spectra ΔA_{ex}^{sim} using the following equation[4]:

$$\Delta A_{ex}^{sim} = (A_{ox} + A_{red}) \cdot \eta - 2 \cdot A_{gr} \cdot (1 - \eta)$$

Luminescence Properties

Fluorescence quantum yields are determined with sample solutions exhibiting an optical density of less than 0.1 at the excitation wavelengths. As standard coumarin 153 in ethanol is applied for excitation wavelengths greater than 380 nm and quinine bisulfate in 0.05 M H_2SO_4 for shorter excitation wavelengths. For coumarin 153 a quantum yield of 53 % and for quinine bisulfate of 52 % is assumed based on the literature.[5,6] The area under the emission spectra recorded for different excitation wavelengths is plotted against the absorbance at the respective excitation wavelength. The slope of the resulting curve is used to calculate the quantum yield according to the following equation:

$$\phi_{Sample} = \Phi_{Standard}\left(\frac{Gradient_{Sample}}{Gradient_{Standard}}\right)\left(\frac{\eta^2_{Sample}}{\eta^2_{Standard}}\right)$$

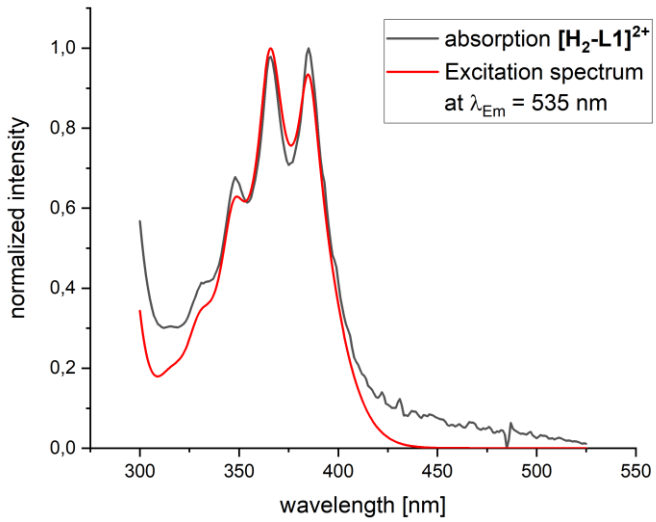

*Figure S 36: Absorption (black) and normalized excitation (red) spectrum of **[H₂-L1]²⁺**. Excitation spectrum showing the intensity of the emission at λ_{em} = 535 nm as function of the excitation wavelength.*

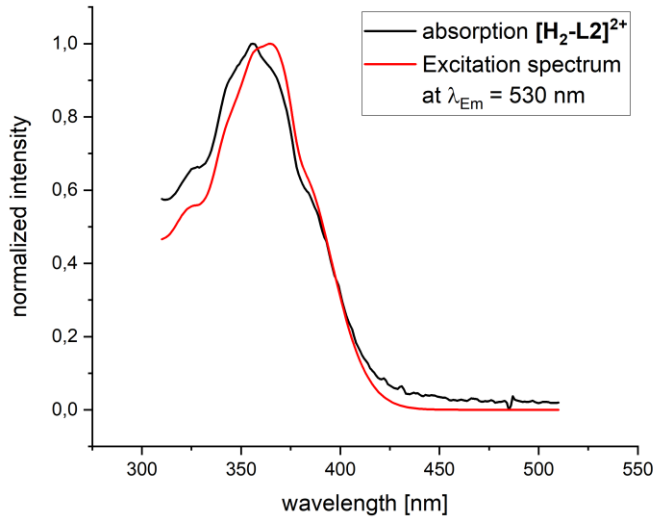

*Figure S 37: Absorption (black) and normalized excitation (red) spectrum of **$[H_2\text{-}L2]^{2+}$**. Excitation spectrum showing the intensity of the emission at λ_{em} = 530 nm as function of the excitation wavelength.*

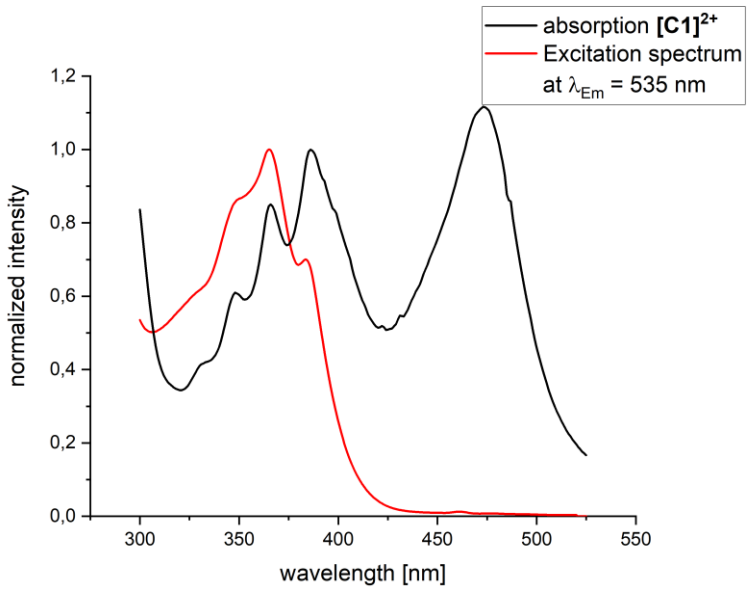

*Figure S 38: Absorption (black) and normalized excitation (red) spectrum of **$[C1]^{2+}$**. Excitation spectrum showing the intensity of the emission at λ_{em} = 535 nm as function of the excitation wavelength.*

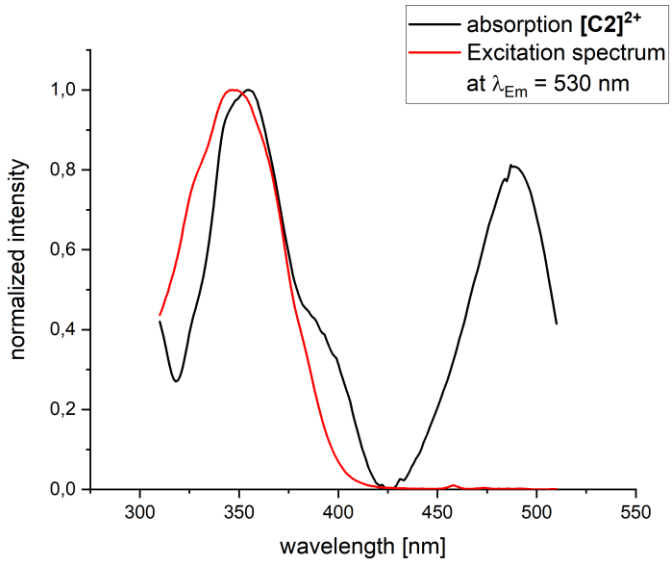

*Figure S 39: Absorption (black) and normalized excitation (red) spectrum of **[C2]²⁺**. Excitation spectrum showing the intensity of the emission at λ_{em} = 530 nm as function of the excitation wavelength.*

Excitation spectra at λ_{Em} = 535 nm reproduce only chromophore part of the spectra in **[H₂-L1]²⁺**, **[H₂-L2]²⁺**, **[C1]²⁺** and **[C2]²⁺**. For **[C1]²⁺** and **[C2]²⁺** the MLCT band in the range of 450 – 500 nm is not reproduced, confirming the assignment of the luminescence to singlet states of the organic chromophores. The MLCT states are not involved in the emission.

Singlet Oxygen Experiments

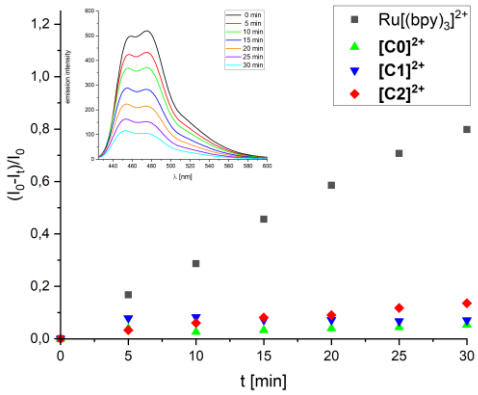

*Figure S 40: **DPBF** consumption as function of irradiation time (λ_{ir} = 480 nm) in air equilibrated MeOH. Inset: time dependent emission spectra of the system with $[Ru(bpy)_3]^{2+}$ as PS, showing the decrease of emission intensity in presence of a long-lived triplet state.*

Black squares represent the consumption of **DPBF** after irradiation with λ_{ir} = 480 nm. $[Ru(bpy)_3]^{2+}$ sensitizes $^1O_2$ with a quantum yield of 0.86.[7] In none of the probed iron complexes **[C0]$^{2+}$-[C2]$^{2+}$** reactive $^1O_2$ was detected after irradiation with λ_{ir} = 480 nm.

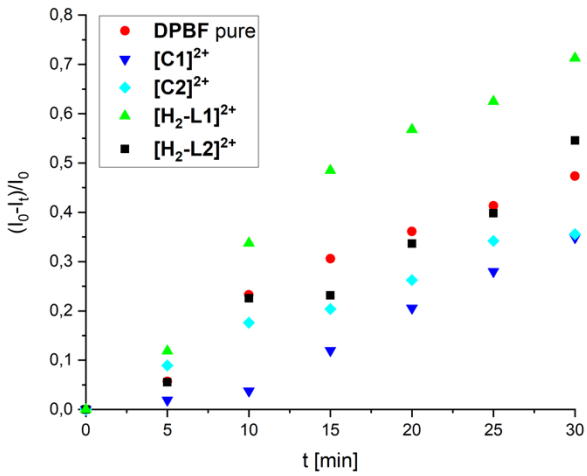

*Figure S 41: **DPBF** consumption as function of irradiation time (λ_{ir} = 346 nm) in air equilibrated MeOH.*

DPBF is not photostable after irradiation with λ_{ir} = 346 nm, therefore the consumption of pure **DPBF** without further photosensitizer is taken as reference. None of the compounds **[H$_2$-L1]$^{2+}$**, **[H$_2$-L2]$^{2+}$**, **[C1]$^{2+}$** and **[C2]$^{2+}$** show a significant difference in the slope of **DPBF** consumption in comparison to pure **DPBF**. This leads to the interpretation, that no long-lived triplet state is populated in **[H$_2$-L1]$^{2+}$**, **[H$_2$-L2]$^{2+}$**, **[C1]$^{2+}$** and **[C2]$^{2+}$** after excitation with λ_{ir} = 346 nm.

References

(1) Möhle, T.; Bokareva, O. S.; Grell, G.; Kühn, O.; Bokarev, S. I. Tuned Range-Separated Density Functional Theory and Dyson Orbital Formalism for Photoelectron Spectra. *Journal of chemical theory and computation* **2018**, *14*, 5870–5880.

(2) Nicholson, R. S.; Shain, I. Theory of Stationary Electrode Polarography. Single Scan and Cyclic Methods Applied to Reversible, Irreversible, and Kinetic Systems. *Anal. Chem.* **1964**, *36*, 706–723.

(3) Randles, J. E. B. A cathode ray polarograph. Part II.—The current-voltage curves. *Trans. Faraday Soc.* **1948**, *44*, 327–338.

(4) Brown, A. M.; McCusker, C. E.; McCusker, J. K. Spectroelectrochemical identification of charge-transfer excited states in transition metal-based polypyridyl complexes. *Dalton transactions (Cambridge, England : 2003)* **2014**, *43*, 17635–17646.

(5) Meech, S. R.; Phillips, D. Photophysics of some common fluorescence standards. *Journal of Photochemistry* **1983**, *23*, 193–217.

(6) Würth, C.; Grabolle, M.; Pauli, J.; Spieles, M.; Resch-Genger, U. Relative and absolute determination of fluorescence quantum yields of transparent samples. *Nature protocols* **2013**, *8*, 1535–1550.

(7) Demas, J. N.; Harris, E. W.; McBride, R. P. Energy transfer from luminescent transition metal complexes to oxygen. *J. Am. Chem. Soc.* **1977**, *99*, 3547–3551.